Rotational stability of dynamic planets with elastic lithospheres

I. Matsuyama,[1,2] J. X. Mitrovica,[3] M. Manga,[4] J. T. Perron,[4] and M. A. Richards[4]

Received 13 April 2005; revised 21 October 2005; accepted 3 November 2005; published 14 February 2006.

[1] We revisit the classic problem of the secular rotational stability of planets in response to loading using the fluid limit of viscoelastic Love number theory. Gold (1955) and Goldreich and Toomre (1969) considered the stability of a hydrostatic planet subject to an uncompensated surface mass load and concluded that a mass of any size would drive true polar wander (TPW) that ultimately reorients the load to the equator. Willemann (1984) treated the more self-consistent problem where the presence of a lithosphere leads to both imperfect load compensation and a remnant rotational bulge. Willemann considered axisymmetric loads and concluded that the equilibrium pole location was governed by a balance, independent of elastic lithospheric thickness, between the load-induced TPW and stabilization by the remnant bulge. Our new analysis demonstrates that the equilibrium pole position is a function of the lithospheric strength, with a convergence to Willemann's results evident at high values of elastic thickness (>400 km for an application to Mars), and significantly larger predicted TPW for planets with thin lithospheres. Furthermore, we demonstrate that nonaxisymmetric surface mass loads and internal (convective) heterogeneity, even when these are small relative to axisymmetric contributions, can profoundly influence the rotational stability. Indeed, we derive the relatively permissive conditions under which nonaxisymmetric forcing initiates an inertial interchange TPW event (i.e., a 90° pole shift). Finally, Willemann's analysis is often cited to argue for a small (<18°) TPW of Mars driven by the development of a Tharsis-sized load. We show that even in the absence of the destabilizing effects of load asymmetry, the equations governing rotational stability permit higher excursions of the Martian rotation vector than has previously been appreciated.

Citation: Matsuyama, I., J. X. Mitrovica, M. Manga, J. T. Perron, and M. A. Richards (2006), Rotational stability of dynamic planets with elastic lithospheres, *J. Geophys. Res.*, *111*, E02003, doi:10.1029/2005JE002447.

1. Introduction

[2] The long-term (secular) rotational stability of terrestrial planets subject to surface mass loading and internal convective dynamics is a long-standing problem in geophysics framed by a series of seminal studies [e.g., *Gold*, 1955; *Goldreich and Toomre*, 1969]. Figure 1 provides a schematic illustration of the basic physical elements that have defined this classic discussion.

[3] *Gold* [1955], for example, discussed the stability of a hydrostatic planet subject to an anomalous (i.e., nonhydrostatic or imperfectly compensated) load (Figures 1a–1c) [see also *Steinberger and O'Connell*, 2002, Figure 1]. The uncompensated load would act to push the rotation pole away (green arrow, Figure 1b) in a reference frame fixed to the load. In the short term, the hydrostatic bulge would act to stabilize the pole (i.e., retard polar motion). However, since the hydrostatic rotational bulge of the planet would, in time, relax to any new orientation of the rotation pole (e.g., Figure 1b), all memory of this previous orientation would ultimately vanish (Figures 1b and 1c). That is, a hydrostatic bulge provides no long-term rotational stability and the reorientation of the pole, or so-called true polar wander (TPW), would be governed solely by the location of the uncompensated surface mass load. In particular, a mass excess of any size (indeed, as small as Gold's beetle) would drive a TPW that would eventually reorient the load to the equator (Figure 1c). Mathematically, the new (final) pole position would be governed by the principal axis of the nonhydrostatic components of the inertia tensor introduced by the uncompensated load. *Gold*'s [1955] arguments were extended by *Goldreich and Toomre* [1969], who demonstrated that a group of anomalous masses moving randomly on the surface (e.g., a set of scurrying beetles) could drive rapid (relative to the speed of the masses) reorientation of the rotation pole.

[4] The *Gold* [1955] analysis, while providing significant insight into the secular rotational stability of planets, in-

[1]Department of Astronomy and Astrophysics, University of Toronto, Toronto, Ontario, Canada.
[2]Now at Department of Terrestrial Magnetism, Carnegie Institution of Washington, Washington, D.C., USA.
[3]Department of Physics, University of Toronto, Toronto, Ontario, Canada.
[4]Department of Earth and Planetary Science, University of California, Berkeley, California, USA.

0148-0227/06/2005JE002447$09.00

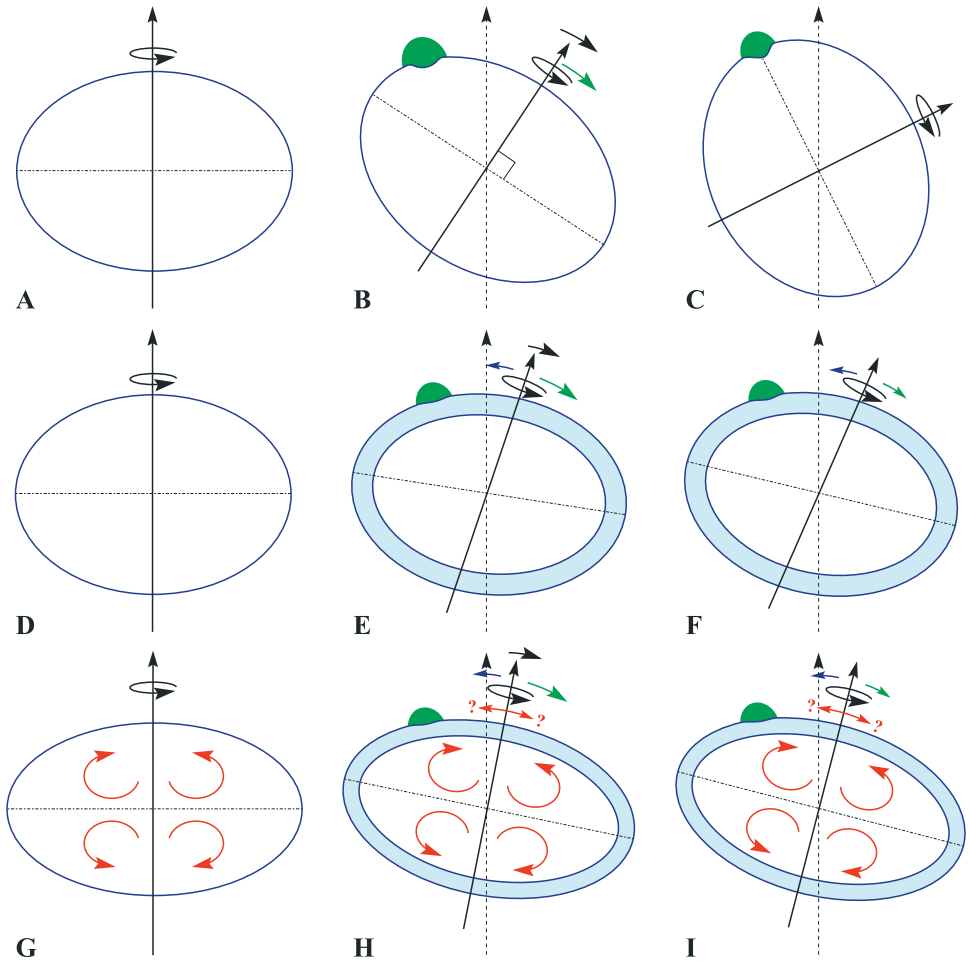

Figure 1. Schematic highlighting some basic physical principles governing, and common approximations applied to, the study of the secular stability of planetary rotation. Figures 1a–1c illustrate arguments described by *Gold* [1955]. An otherwise hydrostatic planet is subject to a surface mass load (the green "beetle") that is at least partially uncompensated. The load pushes the rotation axis away (green arrow) leading to TPW (black arrow) and, after a time period that is long relative to the relaxation of the hydrostatic flattening, the bulge is assumed to perfectly relax to the new pole location (Figures 1b and 1c); there is no memory of the initial pole location. The process continues until the load reaches the planetary equator and TPW ceases. Figures 1d–1f illustrate the extension to *Gold*'s [1955] analysis described by *Willemann* [1984]. In this case, the (uncompensated) load-induced push on the rotation pole is retarded (blue arrow) by the incomplete relaxation of the rotational bulge in the presence of an elastic lithosphere (blue shell). The presence of a remnant rotational bulge is evident in the lack of symmetry of the bulge relative to the rotation axis. The final position of the rotation axis (Figure 1f) is defined by a balance between the load-induced push and the nonhydrostatic remnant bulge stabilization (green and blue arrows, respectively); the load does not, in general, reach the equator (as it does in Figure 1c, where the latter stabilizing effect is absent). Figures 1g–1i extend Figures 1d–1f to consider the potential influence of internal convective dynamics on the rotational state. This impact will depend on the amplitude and (principal axis) orientation of convection-induced perturbations to the inertia tensor (hence the question marks attached to the red arrows in Figures 1h and 1i). The cartoon shows the specific case where convection acts to increase the ellipticity of the rotating planet (compare Figures 1d and 1g); in this case, the "excess" ellipticity will act to stabilize the rotation pole relative to the imposition of the load. The net effect (Figure 1i) is a more subdued TPW relative to the case shown in Figure 1f.

volved an underlying inconsistency that was highlighted, and addressed, by *Willemann* [1984]. The hydrostatic figure is the form achieved by a rotating planet with no elastic (i.e., long-term) strength. Such a form would presumably have been established very early in the planet's history (Figure 1d). Subsequent cooling of the planet and development of a lithosphere would not alter the flattening of this hydrostatic form (Figure 1e); however, the presence of such a lithosphere is the reason why surface mass loads or beetles would not be perfectly compensated. The shortcoming in *Gold*'s [1955] analysis is that the growth of a lithosphere would also ensure that the initial hydrostatic figure of the

planet could not entirely relax to any new orientation associated with TPW (Figures 1e and 1f). Simply put, one cannot have an uncompensated surface mass load and a completely relaxed hydrostatic bulge. This was the central point underlying *Willemann*'s [1984] analysis. In this case, all memory of the original rotation does not vanish, and the ''remnant of the rotational flattening'' [*Willemann*, 1984] will act to stabilize the rotation vector.

[5] What would the final, equilibrium position of the rotation vector be? The final, equilibrium position of the rotation vector is governed by a balance between the TPW driven by the uncompensated component of the load (which acts to move the load to the equator; green line, Figure 1f) and the nonhydrostatic remnant rotational effect (which acts to resist any reorientation of the pole; blue line, Figure 1f). *Willemann* [1984] concluded that the TPW angle will depend on the initial position of the load and its uncompensated size (measured in terms of the degree two geopotential perturbation) relative to the rotational bulge. He furthermore came to the surprising conclusion that the reorientation was independent of the thickness of the lithosphere.

[6] In this paper we revisit the general problem addressed by *Willemann* [1984] using a fluid Love number formulation for the response of the planetary model to surface mass and rotational loading. The analysis makes use of simple, well-documented relationships involving viscoelastic Love number theory [e.g., *Peltier*, 1974; *Mitrovica and Peltier*, 1989], and provides a relatively succinct derivation of the various contributions to the nonhydrostatic inertia tensor. We use our expressions to generalize (and correct) *Willemann*'s [1984] results, to explore a series of important special cases (e.g., the *Gold* [1955] assumption that the hydrostatic bulge relaxes completely in response to a new pole position), and to comment on some more recent analyses of rotational stability which do not appear to have incorporated a remnant rotational bulge [*Bills and James*, 1999].

[7] We complete our analysis by including a separate section that incorporates nonhydrostatic contributions to the inertia tensor driven by internal convective dynamics (Figures 1g–1i). Since the amplitude and orientation of such contributions are unknown for all planets with the possible exception of the Earth, this section is by necessity general (note the question marks in Figure 1i); nevertheless, the expressions we derive will be useful for those interested in the sensitivity of traditional predictions of planetary rotational stability (which focus on external loading) to the presence of potential convective regimes. That such regimes are unconstrained for other planets does not diminish their potential relevance; indeed, it would be difficult to argue that the massive Tharsis rise on Mars, the subject of significant interest in the field of Martian rotation stability [e.g., *Willemann*, 1984; *Bills and James*, 1999], does not reflect the action of both external and internal processes. The existence of the latter will alter the TPW that would be inferred by considering a purely external forcing (compare Figures 1f and 1i).

[8] Following *Willemann* [1984], the analysis described below involves two principal assumptions. First, we adopt spherically symmetric planetary models, and thus any elastic lithospheric lid is treated as uniform (and hence unbroken). Second, we ignore any time history of polar wander and consider only the final, equilibrium position of the pole subsequent to an episode of loading. In practice, the latter, which we will term the ''secular rotational stability,'' implies that the pole position is governed by the principal axis of the nonhydrostatic inertia tensor; thus we circumvent the solution of the time-dependent Liouville equation [e.g., *Ricard et al.*, 1993]. (Another way to interpret this is that we assume that the timescale over which the load acts is very long relative to the bulge and boundary deformation relaxation timescales; this simplifying assumption permits greater clarity in discussing ''before and after,'' or end-member scenarios.) The time required to achieve the final pole position will depend on both the decay times of the planetary modes of viscous relaxation and on the size of the load; in the absence of Willemann's remnant rotational bulge, Gold's beetle will reach the equator, but it may take many billions of years to do so.

2. External Loading

[9] The secular rotational state of the planet is governed by nonhydrostatic variations in the planetary form. In this section we consider perturbations in the inertia tensor, which we denote by I_{ij}, arising from the external loading of the planet. We specify three classes of perturbation associated with: (1) the direct effect of any external surface mass load; (2) the deformation of the planet driven by this surface loading; and (3) incomplete relaxation of the rotational (hydrostatic) flattening due to the presence of a lithosphere.

2.1. Theory

[10] In the following sections we derive expressions for each of these three contributions, making use of Love number theory [*Peltier*, 1974] as well as simple relationships between perturbations in the inertia tensor and the gravitational potential. We will assume that our spherical coordinate system is oriented such that the z axis is fixed to the initial rotation axis of the planet (i.e., prior to loading); in this case, the initial angular velocity vector is given by (0, 0, Ω).

2.1.1. A Mapping Between Gravitational Potential and Inertia Perturbations

[11] Let us assume that a redistribution of mass, either on the surface of the planet or within its interior, gives rise to a perturbation in the gravitational potential, $\mathcal{G}$. We can represent $\mathcal{G}$ in terms of a spherical harmonic decomposition

$$\mathcal{G}(\theta, \phi, t) = \sum_{\ell=0}^{\infty} \sum_{m=-\ell}^{\ell} \mathcal{G}_{\ell m}(t) Y_{\ell m}(\theta, \phi), \tag{1}$$

where θ and ϕ are the colatitude and east longitude, t is time, and the $Y_{\ell m}$ are (complex) surface spherical harmonics. In our derivations, we will normalize these spherical harmonic basis functions such that

$$\int_S Y^{\dagger}_{\ell' m'}(\theta, \phi) Y_{\ell m}(\theta, \phi) dS = 4\pi \delta_{\ell \ell'} \delta_{m m'}, \tag{2}$$

where S represents the surface of the unit sphere and $\delta_{\ell\ell'}$ is the Kronecker delta. Note that $Y_{\ell,-m} = (-1)^m Y^{\dagger}_{\ell m}$, where $\dagger$ represents the complex conjugate.

[12] With this normalization, one can show (e.g., with suitable normalization [*Lambeck*, 1980]) that perturbations to the components of the inertia tensor are related to perturbations in the geopotential by

$$
\begin{aligned}
I_{11}(t) &= \frac{Ma}{g}\left[\frac{2}{3}\mathcal{G}_{00}(t) + \frac{\sqrt{5}}{3}\mathcal{G}_{20}(t) - \sqrt{\frac{10}{3}}\mathrm{Re}(\mathcal{G}_{22}(t))\right],\\
I_{22}(t) &= \frac{Ma}{g}\left[\frac{2}{3}\mathcal{G}_{00}(t) + \frac{\sqrt{5}}{3}\mathcal{G}_{20}(t) + \sqrt{\frac{10}{3}}\mathrm{Re}(\mathcal{G}_{22}(t))\right],\\
I_{33}(t) &= \frac{Ma}{g}\left[\frac{2}{3}\mathcal{G}_{00}(t) - \frac{2\sqrt{5}}{3}\mathcal{G}_{20}(t)\right],\\
I_{12}(t) &= \frac{Ma}{g}\sqrt{\frac{10}{3}}\mathrm{Im}(\mathcal{G}_{22}(t)),\\
I_{13}(t) &= \frac{Ma}{g}\sqrt{\frac{10}{3}}\mathrm{Re}(\mathcal{G}_{21}(t)),\\
I_{23}(t) &= -\frac{Ma}{g}\sqrt{\frac{10}{3}}\mathrm{Im}(\mathcal{G}_{21}(t)),
\end{aligned}
\tag{3}
$$

where M and a are the mass and radius of the planet, respectively, g is the surface gravitational acceleration, and the symbols Re and Im refer to the real and imaginary parts.

2.1.2. Inertia Perturbations: The Surface Mass Load

[13] In this section we focus on predictions of perturbations in the inertia tensor associated with the direct and deformational effects of the surface mass load. As in treatments of post-glacial load-induced variations in the Earth's rotational state (for a new analysis, see *Mitrovica et al.* [2005]), we make the assumption that the planet may be modeled as a spherically symmetric, linear (Maxwell) viscoelastic body and make use of viscoelastic Love number theory.

[14] We begin by denoting an arbitrary surface mass load as $L(\theta, \phi, t)$, with spherical harmonic coefficients given by $L_{\ell m}(t)$. If the mass of the planet is conserved in creating the surface mass load, then $L_{00}(t) = 0$.

[15] Next, we introduce the nondimensional surface load k Love number. In the time domain, this Love number has the form [*Peltier*, 1974, 1976]

$$
k^L_\ell(t) = k^{L,E}_\ell \delta(t) + \sum_{k=1}^{K} r^\ell_k e^{-s^\ell_k t}, \tag{4}
$$

where $\delta(t)$ is the Dirac-delta function. The right-hand side of this expression represents a superposition of an immediate elastic response (note the superscript E) and a nonelastic relaxation governed by a sum of K normal modes of pure exponential decay. These modes are defined by a decay time, $1/s^\ell_k$, and amplitude, r^ℓ_k. We will consider the case where the time elapsed since loading is much longer than the decay times associated with the viscoelastic normal modes in equation (4). That is, all viscous stresses are presumed to have relaxed. In this case, our calculations require the so-called fluid load Love number at spherical harmonic degree two, which we denote by k^L_f. In principle, this number may be computed by taking the Laplace-transform of equation (4) and considering the fluid, $s = 0$ limit to obtain [*Peltier*, 1976]

$$
k^L_f = k^{L,E}_{\ell=2} + \sum_{k=1}^{K} \frac{r^{\ell=2}_k}{s^{\ell=2}_k}. \tag{5}
$$

In practice, the fluid Love number may be accurately computed using a model in which all regions of the planet, with the exception of a purely elastic lithospheric plate, are treated as inviscid [*Peltier et al.*, 1986].

[16] As shown in Appendix A, the load-induced perturbations in the geopotential at degree two can then be written as

$$
\mathcal{G}^L_{2m} = \frac{4\pi a^3 g}{5M} L_{2m} \tag{6}
$$

$$
\mathcal{G}^{L-D}_{2m} = \frac{4\pi a^3 g}{5M} L_{2m} k^L_f. \tag{7}
$$

The superscripts L and $L - D$ represent components associated with the direct mass attraction of the surface load and the deformation induced by this surface load, respectively.

[17] These equations may now be applied to the mapping equation (3). In particular, for a surface load that conserves mass, the total inertia tensor perturbation due to the effects of mass loading,

$$
I^{L,L-D}_{ij} \equiv I^L_{ij} + I^{L-D}_{ij}, \tag{8}
$$

is

$$
\begin{aligned}
I^{L,L-D}_{11} &= 4\pi a^4\left(1 + k^L_f\right)\left[\frac{1}{3\sqrt{5}}L_{20} - \sqrt{\frac{2}{15}}\mathrm{Re}(L_{22})\right],\\
I^{L,L-D}_{22} &= 4\pi a^4\left(1 + k^L_f\right)\left[\frac{1}{3\sqrt{5}}L_{20} + \sqrt{\frac{2}{15}}\mathrm{Re}(L_{22})\right],\\
I^{L,L-D}_{33} &= -\frac{8\pi a^4}{3\sqrt{5}}\left(1 + k^L_f\right)L_{20},\\
I^{L,L-D}_{12} &= \frac{8\pi a^4}{\sqrt{30}}\left(1 + k^L_f\right)\mathrm{Im}(L_{22}),\\
I^{L,L-D}_{13} &= \frac{8\pi a^4}{\sqrt{30}}\left(1 + k^L_f\right)\mathrm{Re}(L_{21}),\\
I^{L,L-D}_{23} &= -\frac{8\pi a^4}{\sqrt{30}}\left(1 + k^L_f\right)\mathrm{Im}(L_{21}),
\end{aligned}
\tag{9}
$$

where the harmonics $L_{\ell m}$ represent the final state of the load (and, once again, after all viscous stresses have relaxed).

[18] When there is no elastic lithosphere, the planet behaves as a purely inviscid material over very long timescales, and the fluid Love number (at spherical harmonic degree two), k^L_f, approaches very close to -1. Thus load-induced perturbations in the inertia tensor vanish ($1 + k^L_f \sim 0$) since the load will be (essentially) perfectly compensated. The existence of a nonzero elastic lithosphere introduces a significant departure from this state since the lithosphere

will provide some (elastic) support for the load (i.e., $1 + k_f^L \neq 0$ [*Wu and Peltier*, 1984]).

2.1.3. Inertia Perturbations: Rotational Effects

[19] The initial, hydrostatic rotational form of a planet will be established during a time when the effective elastic lithospheric thickness is close to zero. As the planet cools, the development over time of an elastic lithosphere of nonzero thickness guarantees that the hydrostatic rotational flattening will never perfectly readjust to a change in the orientation of the rotation pole. In other words, if rotation were to cease, the planet, by virtue of the development of a post-accretion lithosphere, would not assume a spherical form (even in the absence of uncompensated surface loads and internal dynamics). This "partially relaxed remnant of the rotational flattening" [*Willemann*, 1984, p. 703] contributes a nonhydrostatic component to the inertia tensor that serves as the focus of this section.

[20] Following our normalization for the spherical harmonics, the centrifugal potential at the surface of the planet in its initial state is given by

$$\Lambda(\theta, \phi, t) = \Lambda_{00} Y_{00}(\theta, \phi) + \Lambda_{20} Y_{20}(\theta, \phi), \tag{10}$$

where the harmonic coefficients are given by

$$\begin{aligned} \Lambda_{00} &= \frac{a^2 \Omega^2}{3} \\ \Lambda_{20} &= -\frac{a^2 \Omega^2}{3\sqrt{5}}. \end{aligned} \tag{11}$$

[21] The response of the planet to a potential forcing is governed by tidal (or tidal effective) Love numbers. In analogy with equation (4), the time domain form of the viscoelastic tidal k Love number is [*Peltier*, 1974]

$$k_\ell^T(t) = k_\ell^{T,E} \delta(t) + \sum_{k=1}^{K} r'^{\ell}_k e^{-s^\ell_k t}. \tag{12}$$

As in the surface load case, we will be concerned solely with the response of the planet over timescales much longer than the decay times $1/s^\ell_k$; this response is governed by the fluid tidal Love numbers at degree two,

$$k_f^T = k_{\ell=2}^{T,E} + \sum_{k=1}^{K} \frac{r'^{\ell=2}_k}{s^{\ell=2}_k}, \tag{13}$$

and at degree zero,

$$k_{f,0}^T = k_{\ell=0}^{T,E} + \sum_{k=1}^{K} \frac{r'^{\ell=0}_k}{s^{\ell=0}_k}. \tag{14}$$

In this case, the spherical harmonic coefficients of the perturbation to the gravitational equipotential are given by

$$\mathcal{G}^R_{2m} = \Lambda_{2m} k_f^T \tag{15}$$

$$\mathcal{G}^R_{00} = \Lambda_{00} k_{f,0}^T. \tag{16}$$

Equations (3), (11), (15) and (16) can be combined to yield

$$\begin{aligned} I^\Lambda_{11} &= \frac{M\Omega^2 a^3}{9g}\left(2k_{f,0}^T - k_f^T\right), \\ I^\Lambda_{22} &= \frac{M\Omega^2 a^3}{9g}\left(2k_{f,0}^T - k_f^T\right), \\ I^\Lambda_{33} &= \frac{M\Omega^2 a^3}{9g}\left(2k_{f,0}^T + 2k_f^T\right), \\ I^\Lambda_{12} &= I^\Lambda_{13} = I^\Lambda_{23} = 0. \end{aligned} \tag{17}$$

[22] The fluid Love numbers in equation (17) are functions of the elastic lithospheric thickness adopted for the planetary model. In the case where there is no long-term elastic strength in the lithosphere, we will denote the fluid Love numbers as k_f^{T*} (for degree two) and $k_{f,0}^{T*}$ (at degree zero). Using these values in equation (17) yields the hydrostatic form of the planet to the accuracy implied by Love number theory. As we discussed above, the remnant (i.e., nonhydrostatic) rotational flattening associated with the development of an elastic lithosphere is the difference between the rotational forms computed via equation (17) using models with and without an elastic lithosphere. That is,

$$\begin{aligned} I^{ROT}_{11} &= \frac{M\Omega^2 a^3}{9g}\left[2\left(k_{f,0}^{T*} - k_{f,0}^T\right) - \left(k_f^{T*} - k_f^T\right)\right], \\ I^{ROT}_{22} &= \frac{M\Omega^2 a^3}{9g}\left[2\left(k_{f,0}^{T*} - k_{f,0}^T\right) - \left(k_f^{T*} - k_f^T\right)\right], \\ I^{ROT}_{33} &= \frac{M\Omega^2 a^3}{9g}\left[2\left(k_{f,0}^{T*} - k_{f,0}^T\right) + 2\left(k_f^{T*} - k_f^T\right)\right], \\ I^{ROT}_{12} &= I^{ROT}_{13} = I^{ROT}_{23} = 0. \end{aligned} \tag{18}$$

[23] Note that the degree zero contribution to the inertia tensor perturbation is constant for the diagonal elements and zero elsewhere. Hence these degree zero components will yield the inertia tensor of a sphere and thus will have no effect on the orientation and ordering of the principal axes. Accordingly, they do not impact the ultimate reorientation of the pole. We can therefore drop these perturbations to generate the degree-two-only expressions,

$$\begin{aligned} I^{ROT}_{11} &= -\frac{M\Omega^2 a^3}{9g}\left(k_f^{T*} - k_f^T\right), \\ I^{ROT}_{22} &= -\frac{M\Omega^2 a^3}{9g}\left(k_f^{T*} - k_f^T\right), \\ I^{ROT}_{33} &= \frac{2M\Omega^2 a^3}{9g}\left(k_f^{T*} - k_f^T\right), \\ I^{ROT}_{12} &= I^{ROT}_{13} = I^{ROT}_{23} = 0. \end{aligned} \tag{19}$$

[24] We emphasize that our mathematical treatment of the remnant rotational flattening assumes, following the *Willemann* [1984] analysis, a specific sequence of events. In stage I, the hydrostatic form of the planet is established during a period when there is no long-term (elastic) lithospheric strength. This hydrostatic form will perfectly adjust to an arbitrary amount of TPW during stage I. In stage II, an

elastic lithospheric shell develops in response to the cooling of the planet. The theory assumes that this development occurs during a period of no TPW; hence the remnant bulge aligns perfectly with the orientation of the rotational pole within this stage. Finally, in stage III, (internal and/or external) loading drives TPW in the presence of this remnant bulge. The theory can easily be extended to account for a continuous phase of both TPW and lithospheric development prior to loading. In this case, the remnant rotational flattening would be determined via an integration that incorporates slow changes in the lithospheric thickness and any reorientation of the pole (where the integration extends from the formation of the hydrostatic planet to the onset of loading).

2.1.4. Total Inertia Perturbations

[25] An expression for the total inertia tensor perturbation due to the effects of an external surface mass loading,

$$I_{ij}^{L,L-D,ROT} = I_{ij}^{L} + I_{ij}^{L-D} + I_{ij}^{ROT}, \tag{20}$$

can be derived by combining equations (9) and (19),

$$\begin{aligned}
I_{11}^{L,L-D,ROT} &= 4\pi a^4\left(1+k_f^L\right)\left[\frac{1}{3\sqrt{5}}L_{20} - \sqrt{\frac{2}{15}}\mathrm{Re}(L_{22})\right] \\
&\quad - \frac{M\Omega^2 a^3}{9g}\left(k_f^{T*} - k_f^T\right), \\
I_{22}^{L,L-D,ROT} &= 4\pi a^4\left(1+k_f^L\right)\left[\frac{1}{3\sqrt{5}}L_{20} + \sqrt{\frac{2}{15}}\mathrm{Re}(L_{22})\right] \\
&\quad - \frac{M\Omega^2 a^3}{9g}\left(k_f^{T*} - k_f^T\right), \\
I_{33}^{L,L-D,ROT} &= -\frac{8\pi a^4}{3\sqrt{5}}\left(1+k_f^L\right)L_{20} + \frac{2M\Omega^2 a^3}{9g}\left(k_f^{T*} - k_f^T\right), \\
I_{12}^{L,L-D,ROT} &= \frac{8\pi a^4}{\sqrt{30}}\left(1+k_f^L\right)\mathrm{Im}(L_{22}), \\
I_{13}^{L,L-D,ROT} &= \frac{8\pi a^4}{\sqrt{30}}\left(1+k_f^L\right)\mathrm{Re}(L_{21}), \\
I_{23}^{L,L-D,ROT} &= -\frac{8\pi a^4}{\sqrt{30}}\left(1+k_f^L\right)\mathrm{Im}(L_{21}).
\end{aligned} \tag{21}$$

[26] It will be convenient, for the purposes of comparison with previous work (specifically, *Willemann* [1984]), to consider the special case of a disk load with azimuthal symmetry centered at an arbitrary geographic position (θ_L, ϕ_L). Let us say that this load, if centered on the North Pole, was described by spherical harmonic coefficients $L'_{\ell 0}$. Then it is straightforward to show that the harmonic coefficients at degree two for the load centered at (θ_L, ϕ_L) are given by

$$L_{2m} = L'_{20}\frac{Y_{2m}^{\dagger}(\theta_L,\phi_L)}{\sqrt{5}}. \tag{22}$$

The size of the disk load may be conveniently normalized by considering the ratio of the degree two gravitational potential perturbations due to the direct effect of the load and the hydrostatic rotational bulge. If we denote this ratio as Q' (following the symbolism adopted by *Willemann* [1984]), then equations (6), (11), and (15) yield

$$Q' = -\frac{\frac{4\pi a^3 g}{5M}L'_{20}}{\frac{-1}{3\sqrt{5}}a^2\Omega^2 k_f^{T*}}. \tag{23}$$

[27] Using equations (22) and (23) in our expressions for the total inertia perturbation (21) gives

$$\begin{aligned}
I_{11}^{L,L-D,ROT} &= \frac{1}{3}m'\left\{Q'\alpha\left[\frac{1}{\sqrt{5}}Y_{20}(\theta_L) - \sqrt{\frac{6}{5}}\mathrm{Re}\left(Y_{22}^{\dagger}(\theta_L,\phi_L)\right)\right] - 1\right\}, \\
I_{22}^{L,L-D,ROT} &= \frac{1}{3}m'\left\{Q'\alpha\left[\frac{1}{\sqrt{5}}Y_{20}(\theta_L) + \sqrt{\frac{6}{5}}\mathrm{Re}\left(Y_{22}^{\dagger}(\theta_L,\phi_L)\right)\right] - 1\right\}, \\
I_{33}^{L,L-D,ROT} &= -\frac{2}{3}m'\left[Q'\alpha\frac{1}{\sqrt{5}}Y_{20}(\theta_L) - 1\right], \\
I_{12}^{L,L-D,ROT} &= \frac{1}{3}m'Q'\alpha\sqrt{\frac{6}{5}}\mathrm{Im}\left(Y_{22}^{\dagger}(\theta_L,\phi_L)\right), \\
I_{13}^{L,L-D,ROT} &= \frac{1}{3}m'Q'\alpha\sqrt{\frac{6}{5}}\mathrm{Re}\left(Y_{21}^{\dagger}(\theta_L,\phi_L)\right), \\
I_{23}^{L,L-D,ROT} &= -\frac{1}{3}m'Q'\alpha\sqrt{\frac{6}{5}}\mathrm{Im}\left(Y_{21}^{\dagger}(\theta_L,\phi_L)\right),
\end{aligned} \tag{24}$$

where

$$m' = \frac{1}{3}\frac{M\Omega^2 a^3}{g}\left(k_f^{T*} - k_f^T\right) \tag{25}$$

$$\alpha = \frac{1+k_f^L}{1-k_f^T/k_f^{T*}}. \tag{26}$$

[28] Note that the values m' and α only involve parameters associated with the planetary model (fluid Love numbers, radius, mass, rotation rate). The size of the load is embedded in Q' and its location governs the evaluation of the surface spherical harmonics Y_{2m} in equation (24).

[29] As one further simplification to the equations for the inertia tensor perturbations, we can assume, with no loss of generality, that the load is placed along the great circle of zero longitude ($\phi_L = 0$). In this case,

$$\begin{aligned}
I_{11}^{L,L-D,ROT} &= \frac{1}{3}m'\left\{Q'\alpha\left[P_{20}(\theta_L) - \frac{1}{2}P_{22}(\theta_L)\right] - 1\right\}, \\
I_{22}^{L,L-D,ROT} &= \frac{1}{3}m'\left\{Q'\alpha\left[P_{20}(\theta_L) + \frac{1}{2}P_{22}(\theta_L)\right] - 1\right\}, \\
I_{33}^{L,L-D,ROT} &= -\frac{2}{3}m'[Q'\alpha P_{20}(\theta_L) - 1], \\
I_{13}^{L,L-D,ROT} &= \frac{1}{3}m'Q'\alpha P_{21}(\theta_L), \\
I_{12}^{L,L-D,ROT} &= I_{23}^{L,L-D,ROT} = 0,
\end{aligned} \tag{27}$$

where the P_{2m} refer to unnormalized Legendre polynomials ($P_{20}(\theta) = (3\cos^2\theta - 1)/2$; $P_{21} = -3\sin\theta\cos\theta$; $P_{22} = 3\sin^2\theta$).

2.1.5. *Willemann* [1984] Revisited

[30] Equation (27) can be directly compared with the derivation by *Willemann* [1984] for inertia tensor perturba-

tions due to external surface mass loading. His results (see equations (21–24)) are

$$
\begin{aligned}
I_{11}^{L,L-D,ROT} &= \frac{1}{3}m''\left\{Q'\left[P_{20}(\theta_L)-\frac{1}{2}P_{22}(\theta_L)\right]-1\right\},\\
I_{22}^{L,L-D,ROT} &= \frac{1}{3}m''\left\{Q'\left[P_{20}(\theta_L)+\frac{1}{2}P_{22}(\theta_L)\right]-1\right\},\\
I_{33}^{L,L-D,ROT} &= -\frac{2}{3}m''[Q'P_{20}(\theta_L)-1],\\
I_{13}^{L,L-D,ROT} &= \frac{1}{3}m''Q'P_{21}(\theta_L),\\
I_{12}^{L,L-D,ROT} &= I_{23}^{L,L-D,ROT}=0,
\end{aligned}
\tag{28}
$$

where

$$
m'' = \frac{1}{2}\frac{M\Omega^2 a^3}{g}(1-c) \tag{29}
$$

and c is "the degree of compensation of a load" [*Willemann*, 1984, p. 703] (see discussion below).

[31] There are two notable differences between our equation (27) and equation (28). First, the parameters m' and m'' differ by a factor of 3/2. This factor arises because of an error in *Willemann*'s [1984] expressions for the degree two, order zero potential perturbations associated with both the mass loading and the remnant of the rotational flattening. Since the error is the same for all components of the inertia tensor, it has no effect on the determination of the principal axes and, thus, the orientation of the rotation axis.

[32] A second, more important difference is manifest both in the absence of the term α in equation (28) and in a second difference between the parameters m' and m''. In regard to the latter, m' includes the factor $k_f^{T*} - k_f^T$, while m'' has $(1 - c)$. These differences are a consequence of *Willemann*'s [1984] assumption that at degree two the planetary response to a surface mass load is identical to the response to a potential forcing. While *Willemann* [1984] did not adopt a Love number terminology for the load response, his value of c is identical to $-k_f^L$, and thus the term $(1 - c)$ in equation (29) can be replaced by $(1 + k_f^L)$. His assumption that the response to a mass load and potential forcing are equivalent is, in Love number terminology, the same as assuming that $k_f^T = - k_f^L$ (and therefore that $k_f^{T*} = - k_f^{L*}$). If one notes that k_f^{L*} is equal to -1 because a load on a planet with no elastic lithosphere will ultimately be perfectly compensated, then *Willemann*'s [1984] assumption applied to equation (27) leads to $\alpha = 1$ and $k_f^{T*} - k_f^T = 1 + k_f^L$. That is, equation (28) is obtained.

[33] The error within the term m'' introduced by this assumption is of no consequence since it impacts all the inertia components by the same factor. However, the error introduced by assuming that $\alpha = 1$ will impact the calculated orientation of the rotation pole. This error will, moreover, be dependent on the planetary model, specifically, the density structure and the thickness and rigidity of the elastic lithosphere. *Willemann* [1984] concluded that the reorientation of the planetary rotation axis in response to a surface mass load is independent of the lithospheric thickness (LT). This is incorrect. The corrected theory (27), and in particular the appearance of the term α, introduces a dependence on LT, and, more generally, on the detailed internal structure of the planet (since the fluid Love numbers depend on both).

2.2. Results

[34] The long-term, equilibrium, orientation of the rotation vector is governed by the principal axis of the nonhydrostatic inertia tensor. In this section we use the expressions for the latter derived above to evaluate TPW driven by surface mass loading under a variety of illustrative cases.

2.2.1. Axisymmetric Loads

[35] We start with the special case treated by *Gold* [1955] and *Goldreich and Toomre* [1969]: a "quasi-rigid" planetary model in which the surface load (beetle) is not entirely compensated by deformation, while the rotational bulge is able to fully relax to any reorientation of the pole (and thus provides no long-term resistance to TPW). If we adopt the simplified expressions appropriate for an axisymmetric disk load emplaced on the great circle $\phi_L = 0$ (equation 27), and ignore the terms associated with the fossil rotational bulge, then the nonhydrostatic inertia tensor for this special "quasi-rigid" case is given by

$$
\begin{aligned}
I_{11}^{L,L-D} &= \frac{1}{3}m'Q'\left(1+k_f^L\right)\left[P_{20}(\theta_L)-\frac{1}{2}P_{22}(\theta_L)\right],\\
I_{22}^{L,L-D} &= \frac{1}{3}m'Q'\left(1+k_f^L\right)\left[P_{20}(\theta_L)+\frac{1}{2}P_{22}(\theta_L)\right],\\
I_{33}^{L,L-D} &= -\frac{2}{3}m'Q'\left(1+k_f^L\right)P_{20}(\theta_L),\\
I_{13}^{L,L-D} &= \frac{1}{3}m'Q'\left(1+k_f^L\right)P_{21}(\theta_L),\\
I_{12}^{L,L-D} &= I_{23}^{L,L-D}=0.
\end{aligned}
\tag{30}
$$

If we define δ as the TPW angle (i.e., the angle between the initial and final rotation axis, where TPW away from the load is taken as positive), then one can show, after some algebra, that the diagonalization of the nonhydrostatic inertia tensor defined by equation (30) yields

$$
\delta = \begin{cases} \frac{\pi}{2}-\theta_L & Q'>0 \\ -\theta_L & Q'<0. \end{cases} \tag{31}
$$

The final colatitude of the load, which we will denote by θ_L^f, is given by $\delta + \theta_L$. Thus a mass excess ($Q' > 0$) will drive a TPW that brings the load onto the equator (regardless of the size of Q') relative to the final pole location (i.e., $\theta_L^f = \delta + \theta_L = \pi/2$). Physically, the uncompensated surface mass load will move to the equator without any long term resistance (in this special, "quasi-rigid" case) from a remnant rotational bulge. (As discussed in section 1, the time required to reach this final state will depend on the size of the load and the decay times of the planetary modes of relaxation.) This is, of course, a classic result in rotational dynamics [*Gold*, 1955] (Figures 1a–1c), and it leads to a second equally seminal result [*Goldreich and Toomre*, 1969], namely that a set of mass loads moving randomly on the surface can drive large changes in the orientation of the pole with a timescale that may be fast relative to the motion of the surface masses. For completeness, we note that TPW driven by a surface mass deficit (i.e., $Q' < 0$) on a "quasi-

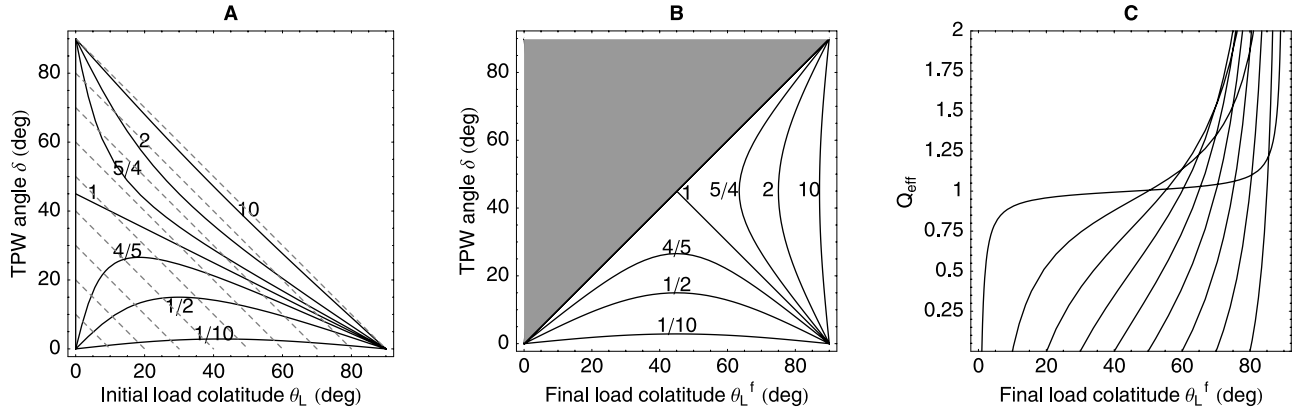

Figure 2. TPW solutions based on equations (34) and (35). (a) Solid lines denote TPW angle, δ, versus initial colatitude of the surface mass load, θ_L, for a suite of different values of the effective load size, Q_{eff} (as labeled). Dashed lines join (δ, θ_L, Q_{eff}) solutions with a common final load colatitude, θ_L^f. These lines begin at $\theta_L^f = 10°$ at bottom left and increase in increments of 10° (up to $\theta_L^f = 90°$). (b) TPW angle, δ, versus final load location, θ_L^f, for the same set of Q_{eff} values shown in Figure 2a. The shaded region at top left masks physically impossible solutions in which the TPW angle is greater than the final load location. (c) Relationship between Q_{eff} and the final load colatitude, θ_L^f, for different values of the initial load location, θ_L. The value of the latter for each of the lines on the figure can be inferred from the $Q_{eff} = 0$ intercept (i.e., when $Q_{eff} = 0$ the pole does not reorient and therefore the initial and final load locations are the same).

rigid'' planet will act to bring the load onto the pole (case two in equation (31); $\theta_L^f = 0$).

[36] Next, we move to the more general case where the presence of an elastic lithospheric shell leads, in addition to an imperfect compensation of the surface mass load, to the incomplete relaxation of the rotational bulge. This was the problem addressed by *Willemann* [1984]. For the axisymmetric disk load applied on the great circle $\phi_L = 0$, equation (27) provides expressions for the nonhydrostatic inertia elements in this case. As a first step, diagonalization of these elements yields (again, after some algebra)

$$\begin{aligned} I_{11}^{L,L-D,ROT} &= \frac{1}{3}m'\left[Q'\alpha\left(3\cos^2\theta_L^f - 2\right) - 3\cos^2\delta + 2\right], \\ I_{22}^{L,L-D,ROT} &= \frac{1}{3}m'(Q'\alpha - 1), \\ I_{33}^{L,L-D,ROT} &= -\frac{1}{3}m'\left[Q'\alpha\left(3\cos^2\theta_L^f - 1\right) - 3\cos^2\delta + 1\right], \end{aligned} \tag{32}$$

$$\begin{aligned} I_{13}^{L,L-D,ROT} &= \frac{1}{2}m'\left[-Q'\alpha\sin\left(2\theta_L^f\right) + \sin(2\delta)\right], \\ I_{12}^{L,L-D,ROT} &= I_{23}^{L,L-D,ROT} = 0, \end{aligned} \tag{33}$$

where δ is the TPW angle that diagonalizes the inertia tensor. This diagonalization process is completed by setting $I_{13} = 0$, which gives

$$\delta = \frac{1}{2}\arcsin\left[Q'\alpha\sin\left(2\theta_L^f\right)\right], \tag{34}$$

or, in terms of the initial load colatitude,

$$\delta = \frac{1}{2}\arctan\left[\frac{Q'\alpha\sin(2\theta_L)}{1 - Q'\alpha\cos(2\theta_L)}\right]. \tag{35}$$

[37] As would be expected from the discussion in the last section, equation (34) is identical to *Willemann*'s [1984] result (see his equation (28)) with the exception that our $Q'\alpha$ replaces Q'. We will emphasize this connection by defining $Q_{eff} \equiv Q'\alpha$.

[38] The final location of the pole in this general case is governed by a balance (see Figures 1d–1f) between the load-induced TPW highlighted above (which acts to move a mass excess to the equator and a mass deficit to the pole) and the stabilizing effect of the remnant rotational flattening (which acts to resist any reorientation of the pole away from its initial location). Under *Willemann*'s [1984] assumption that the load and rotational forcing are subject to the same level of compensation ($\alpha = 1$), the level of TPW which achieves this balance is independent of the lithospheric thickness. The appearance of α in equation (34) (and 27) alters the TPW with which this balance is achieved; since α is a function of the thickness and rigidity of the lithosphere as well as the planetary density structure, so too will be the predicted TPW.

[39] Figure 2 plots various families of solutions to equation (34) as a function of the TPW angle δ, Q_{eff}, the initial load co-latitude (θ_L) and the final load colatitude (θ_L^f). Figure 2a (solid lines), for example, shows calculations of δ versus the initial colatitude of the surface mass load for a suite of different values of Q_{eff} (since $Q_{eff} > 0$, we are assuming in all cases a mass excess). The dashed lines in this frame join solutions with the same final load colatitude. In contrast, Figure 2b shows δ as a function of final load colatitude for the same suite of Q_{eff} values; note, in this case, that results for $Q_{eff} = x$ and $1/x$ are symmetrical around the $Q_{eff} = 1$ solution. Finally, Figure 2c plots Q_{eff} versus θ_L^f for a suite of different initial load locations (see caption). This plot makes it simple to assess how high Q_{eff} must be to attain a final load location for a specific starting location.

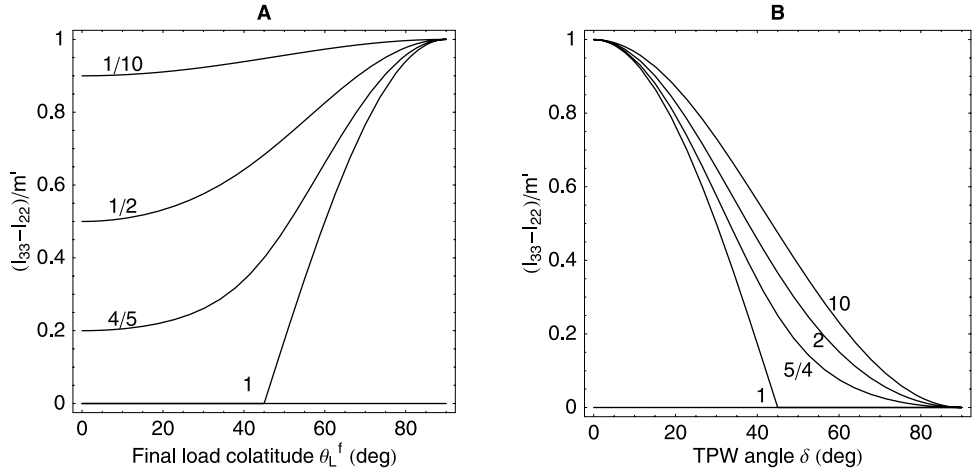

Figure 3. Difference between the two largest dimensionless principal moments $(I_{33} - I_{22})/m'$ for a suite of different values of the effective load size, Q_{eff} (as labeled), (a) as a function of the final load colatitude, θ_L^f, for $Q_{eff} \leq 1$, and (b) as a function of the TPW angle, δ, for $Q_{eff} \geq 1$.

[40] When $Q_{eff} = 1$, the TPW angle δ is identical to the angle from the final equator to the load (i.e., the final latitude of the load); that is, reorientation of the pole is equal to the residual distance between the load and the equator. Mathematically, $\delta = \pi/2 - \theta_L^f$, which is clear from the $Q_{eff} = 1$ solution on Figure 2b. As $Q_{eff} \rightarrow \infty$, the uncompensated load dominates any remnant rotational bulge and the final load location approaches the equator. Conversely, when $Q_{eff} \rightarrow 0$, the remnant rotational bulge dominates and the pole is negligibly perturbed by the surface loading. (Both limits are evident on each of the frames on the figure.)

[41] The results for $Q_{eff} = 1$ and $\theta_L = 0$ are worthy of further comment. In this case alone, the degree two component of the compensated load "cancels" the remnant rotational bulge and all inertia perturbations in equation (33) will be zero (note that when $\theta_L = 0$, θ_L^f is the same as δ). Thus the polar motion will be undefined since there is no principal axis orientation, and this is reflected in our vertical solid line at $\theta_L = 0$ in Figure 2a. Since the orientation of the remnant bulge is governed by the initial rotation axis, this cancellation is only possible when $\theta_L = 0$.

[42] This special case provides one explanation for the clustering of the $Q_{eff} > 1$ and, separately, the $Q_{eff} < 1$ solutions when $\theta_L \sim 0$ in Figure 2a. In particular, consider a value of $Q_{eff} = 1 + \epsilon$. The first term on the RHS of this expression may be interpreted as that portion of Q_{eff} which will cancel the inertia perturbation associated with the remnant rotational effect (when $\theta_L = 0$). Thus the sign of ϵ will govern the final position of the pole: If $\epsilon > 0$, there will be a mass excess at the pole (relative to the remnant rotational bulge) and, regardless of the magnitude of this excess (that is, the size of ϵ), the load will ultimately move to the equator (i.e., all $Q_{eff} > 1$ solutions cluster at $\delta = 90°$ when $\theta_L \sim 0$); alternatively, if $\epsilon < 0$, there will be a mass deficit at the pole and the load will stay at the pole (i.e., all $Q_{eff} < 1$ solutions cluster at $\delta = 0°$ when $\theta_L \sim 0$).

[43] In the parlance of rotation theory, the 90° shift in the rotation pole when $Q_{eff} > 1$ and $\theta_L = 0$ is a so-called inertial interchange true polar wander (IITPW) event [*Goldreich and Toomre*, 1969]. Such instabilities occur when the (diagonalized) maximum and intermediate nonhydrostatic inertia elements are exchanged by any process. In our case, we have chosen $\phi_L = 0$, $I_{22} > I_{11}$, and thus the IITPW condition becomes $I_{22} \geq I_{33}$. Using equation (33), this condition may be written as: $Q_{eff} \cos^2 \theta_L^f \geq \cos^2 \delta$. However, for $\theta_L = 0$, $\theta_L^f = \delta$, and therefore the IITPW condition is simply $Q_{eff} \geq 1$, as we discussed above.

[44] In the absence of a remnant rotational bulge a beetle of arbitrary size will move to the equator [*Gold*, 1955]. For a planet with a lithosphere this level of rotational instability will occur in two special cases: (1) when $Q_{eff} \gg 1$, and thus the size of the load is sufficiently large that the remnant bulge becomes inconsequential; and (2) when the (axisymmetric) load is placed near the initial rotation pole ($\theta_L = 0$) and it has a (degree two) amplitude in excess of the bulge signal ($Q_{eff} > 1$).

[45] The above discussion of rotational stability may also be summarized, quantitatively, by considering the variation in the individual principal moments of inertia as a function of parameters governing load location. In Figure 3, we show the difference $(I_{33} - I_{22})/m'$ as a function of final load colatitude θ_L^f for $Q_{eff} \leq 1$ and as a function of TPW angle δ for $Q_{eff} \geq 1$. (The change in the abscissa for Q_{eff} less than or greater than 1 reflects the nature of the results in Figure 2b; for each $Q_{eff} \leq 1$ there are two solutions for a given δ, while for each $Q_{eff} \geq 1$ there are two solutions for a given θ_L^f.) The figure demonstrates that for $Q_{eff} < 1$, the maximum and intermediate moments do not cross, and that the difference $I_{33} - I_{22}$ grows (i.e., the rotational stability increases) as Q_{eff} is reduced. In contrast, for $Q_{eff} \geq 1$, these principal moments do cross as δ approaches 90°, reflecting the conditions for an IITPW event.

[46] The family of solid lines in Figure 2a are identical to *Willemann*'s [1984] curves showing δ versus Q' (rather than Q_{eff}) and the question arises as to how much Q' and Q_{eff} may differ (or, equivalently, to what extent the Love number factor α may diverge from 1). To explore this issue we consider, as an illustrative example, the case of Mars. Using standard procedures [*Peltier et al.*, 1986], we have computed fluid load and tidal Love numbers for the simple five-layer model of Martian structure described by *Bills and*

Table 1. Effects of Lithospheric Thickness Upon the Mars Model Parameters[a]

LT, km	k_f^L	k_f^T	$\alpha = \frac{1+k_f^L}{1-k_f^T/k_f^{T*}}$	$\beta = \frac{1}{1-k_f^T/k_f^{T*}}$
50	−0.91643	1.1087	1.2708	15.206
100	−0.85285	1.0373	1.1686	7.9418
200	−0.69063	0.84749	1.0822	3.4982
300	−0.57531	0.71240	1.0625	2.5019
400	−0.48769	0.60973	1.0537	2.0567

[a]LT denotes lithospheric thickness. The tidal fluid Love number for LT = 0 is $k_f^{T*} = 1.1867$.

James [1999]. These values, together with the factor α (equation (26)) are provided in Table 1 for a sequence of elastic LT ranging from 50 km to 400 km. Note that α diverges monotonically from 1 for progressively lower values of lithospheric thickness, reaching a value of 1.27 for the case LT = 50 km.

[47] Ultimately, applying the rotational stability theory described here to a specific loading event requires some estimate of the Q' associated with the loading; that is, following equation (23), an estimate of the size of the uncompensated load relative to the rotational bulge of the planet. However, the TPW angle is governed by the parameter Q_{eff} (equation (34)). In the case of the model of Mars used to generate Table 1, *Willemann*'s [1984] theory underestimates Q_{eff} by (for example) 27% for the case LT = 50 km, and 17% for LT = 100 km. To explore the impact of this discrepancy on the predicted TPW, consider Figure 4. The figure shows the computed TPW angle versus the final load location (as in Figure 2b) for the case of $Q' = 1.74$ and α values appropriate to the cases of LT = 50 km, 100 km, 200 and 400 km in Table 1. Also shown in the figure (dashed line) is the (LT-independent) solution associated with *Willemann*'s [1984] theory ($Q' = 1.74$ and $\alpha = 1$). We adopt the value of $Q' = 1.74$ because it is the upper bound value inferred by *Willemann* [1984] for the loading of Mars by the Tharsis volcanic province; in this regard, the figure is limited to θ_L^f values (80–90°) that span estimates for the central colatitude of Tharsis.

[48] Figure 4 raises a number of interesting issues. First, *Willemann* [1984] has been cited as one argument against significant TPW driven by Tharsis loading [e.g., *Grimm and Solomon*, 1986; *Banerdt et al.*, 1992; *Ward*, 1992; *Zuber and Smith*, 1997]. Indeed, *Willemann* [1984] concluded that the reorientation was "certainly less than 18°." However, on the basis of Willemann's theory, a present location of Tharsis at 80–90° colatitude is consistent with a TPW event of either $\delta < 18°$ or $\delta > 72°$. (These two solutions are also evident within the $80° < \theta_L^f < 90°$ portion of Figure 2b; the physics associated with the latter, large TPW event was described in detail above.) *Willemann* [1984] dismissed the latter range because it implies an initial load location within 8° of the rotation pole (since the $\delta = 72°$ TPW solution yields a final load location at 80°); he considered this to be unlikely relative to a $\delta < 18°$ solution that implies an initial load location greater than 62° from the pole. This argument (which appears to discount, a priori, any large TPW event) is independent of the physics governing the rotational stability (Figures 2b and 4), and we do not find it compelling.

[49] As expected from Table 1, predictions based on our new theory (equation (34)) converge to *Willemann*'s [1984] solution for the thick lithosphere cases (LT = 300 or 400 km). In contrast, the LT = 50 km predictions are significantly different from this solution. In this case, we would conclude that a final Tharsis colatitude between 80° and 90° is consistent with a reorientation of the rotation pole of either $\delta < 25°$ or $\delta > 65°$. The latter solution, which implies an initial load location within 15° of the pole, would be consistent with a large TPW event suggested by some studies [e.g., *Schultz and Lutz*, 1988; *Arkani-Hamed and Boutin*, 2004; *Arkani-Hamed*, 2005].

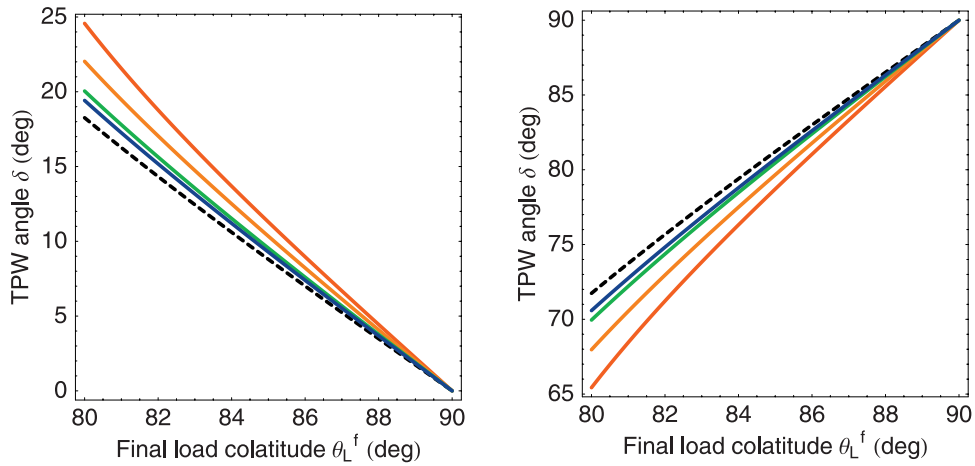

Figure 4. TPW angle, δ, versus the final load colatitude, θ_L^f, for the specific load size $Q' = 1.74$. The figure only shows the range $80° < \theta_L^f < 90°$. In this case, two solutions are evident with TPW angles near (left) 20° and (right) 70°. On each frame, the lines refer to solutions with lithospheric thickness (LT) of 50 km (red), 100 km (orange), 200 km (green), and 400 km (blue); the value of α for each of these models is given in Table 1. Also shown (dashed line) is the solution based on *Willemann*'s [1984] theory (which is independent of LT).

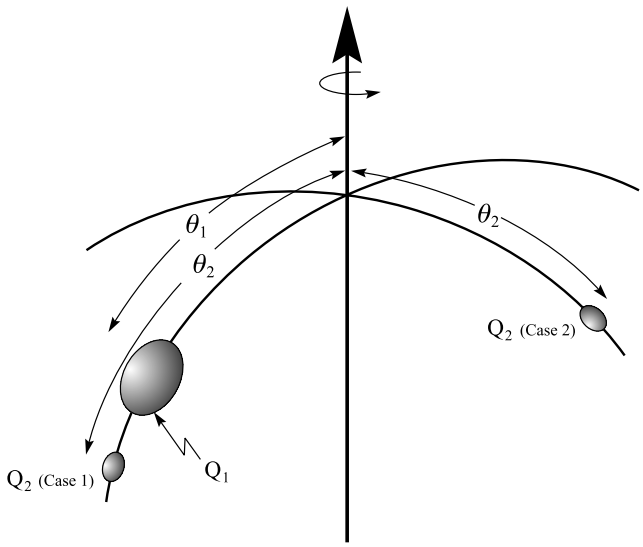

Figure 5. Schematic illustration of the initial orientation of the nonaxisymmetric surface mass load discussed within the text. In particular, the central, axisymmetric load of size Q_1 and initial colatitude θ_1 (as in Figures 2 and 3) is augmented to include a smaller second disk of size Q_2. The latter is positioned either on the great circle joining the central disk to the initial pole (Case 1) or 90° from this great circle (Case 2).

[50] Table 1 suggests that the divergence between our results and those derived from *Willemann*'s [1984] theory will continue as the lithosphere is further thinned and thus that there will be a marked trend toward greater rotational instability for planets with progressively thinner elastic shells. Applying the rotational stability theory to the loading of Mars by Tharsis raises an important issue; namely, the LT used in the theory refers to the thickness of the lithosphere at the time of Tharsis development. This thickness is uncertain, particularly given the ancient nature of Tharsis (~4 Ga). As we discussed at the end of section 2.1.3, the remnant rotational flattening active at the time of Tharsis loading should actually reflect, in an integral sense, changes in both the pole position and lithospheric thickness across a time interval from the formation of the hydrostatic planet to the onset of Tharsis loading; the TPW calculations above (and those appearing in the work of *Willemann* [1984]) assume that the lithospheric thickness at the time of Tharsis loading developed during a period of little TPW and thus the remnant bulge is aligned with the unique orientation of the pole during this period.

2.2.2. *Bills and James* [1999]

[51] In application to Mars, *Bills and James* [1999] also considered the rotational stability of the planet in response to surface mass loading. Their equation governing the secular rotational stability was stated as (see their equation (49))

$$J_2^L \geq 2J_{22}^L, \tag{36}$$

where J_2^L and J_{22}^L represent the degree two zonal and nonzonal components of the potential perturbation associated with the surface mass load. These harmonics are renormalized versions of the coefficients appearing in equation (1). This stability criterion is identical to

$$I_{33}^L + I_{33}^{L-D} \geq I_{22}^L + I_{22}^{L-D}, \tag{37}$$

where each side of this equation represents a principal axis. That is, *Bills and James* [1999] assume that the pole location is governed by the diagonalization of a nonhydrostatic inertia tensor whose sole contribution arises from surface mass loading. The stabilization of the pole due to a remnant rotational bulge is ignored.

[52] *Bills and James* [1999] were, in particular, interested in the impact on the rotational state of departures from load axial symmetry. This issue is the subject of the next section.

2.2.3. Nonaxisymmetric Loads

[53] Thus far we have only considered simple, axisymmetric disk loads. To end this section we explore the potential impact on the rotational stability of any departures from axisymmetry. Specifically, we will consider TPW driven by the spherical harmonic degree two components of the simple set of disks shown schematically in Figure 5. The total load is composed of two parts. The first, axisymmetric central dome has an uncompensated, effective load size of Q_1. The second, smaller disk has an uncompensated, effective size of Q_2. We will consider two cases distinguished on the basis of the location of this smaller disk: either on the great circle joining the initial rotation pole and the larger disk (Case 1) or 90° from this great circle (Case 2). To this point we have been concerned with computing the TPW angle δ along this great circle. The natural question that arises is the following: How effective is the nonaxisymmetric component of the surface load in driving TPW off this great circle? Since no real load (or set of loads) is perfectly axisymmetric, Tharsis being a notable example, this question has important relevance to any general consideration of rotational stability.

[54] To consider this issue, we have performed a suite of calculations in which we adopt a specific initial load location θ_1 close to the initial rotation axis and fix Q_2 to some small fraction of Q_1. We then track the computed TPW while varying the central load amplitude Q_1. These solutions map out a curve on the surface of the sphere. We have repeated the calculation for various placements of the secondary disk.

[55] In these tests, which we summarize in Figures 6 and 7, the TPW is driven by three contributions to the planetary inertia tensor, where each contribution has its preferred pole location: the fossil rotational bulge acts to move the pole toward the original pole location, while the two surface mass loads drive the pole toward great circles perpendicular to the respective load location vectors (these great circles are given by the solid red and blue lines in Figures 6 and 7). The equilibrium pole location is given by the balance of these three contributions.

[56] As an example, the top row of Figure 6 shows calculations for the Case 1 orientation of the secondary load disk when $\theta_1 = 1°$ and $\theta_2 = 11°$ (or 10° further from the initial pole than the primary disk). As Q_1 is increased from zero to values just above 1, the TPW solutions move along

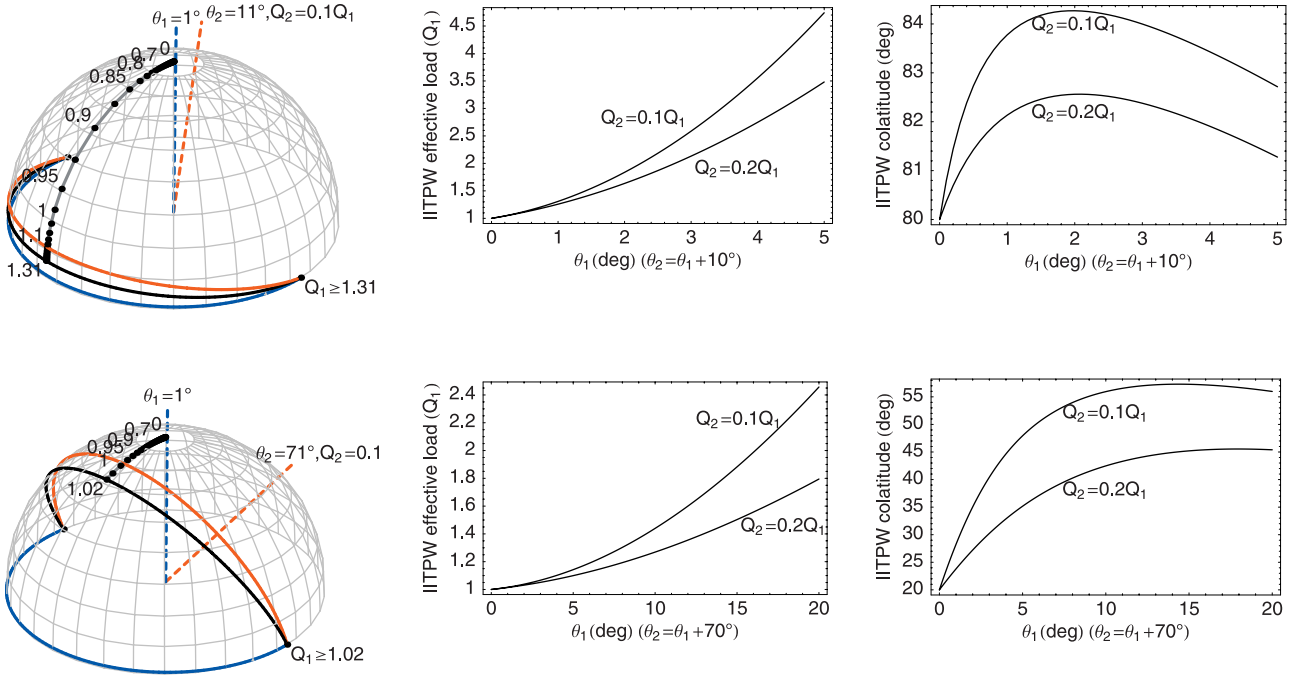

Figure 6. Predicted TPW for the nonaxisymmetric load scenario shown by Case 1 in Figure 5 (i.e., the secondary load falls on the great circle connecting the initial pole location to the primary load). (top left) Predicted TPW for a suite of predictions based on varying the effective size of the primary load, Q_1 (as labeled). In this case $\theta_1 = 1°$, $\theta_2 = 11°$ and $Q_2 = 0.1\ Q_1$. The blue and red great circle arcs are perpendicular to the axes of the primary and secondary loads, respectively. An IITPW event occurs for $Q_1 = 1.31$ and the rotation pole moves to the intersection of the blue and red great circles (i.e., 90° from both the primary and secondary loads; given the symmetry of the problem, the pole can move either clockwise or counterclockwise during this event, hence the two paths shown on the figure). (top middle and right) The effective primary load, Q_1, required to produce an IITPW event, as well as the colatitude of the pole when this event is initiated, as a function of the initial load colatitude, θ_1. Each frame shows results for two scenarios: $Q_2 = 0.1\ Q_1$ and $Q_2 = 0.2\ Q_1$. (bottom) As in the top row, except for the case where the secondary load is displaced 70° from the primary load. In this case, the middle and right frames explore results for θ_1 values up to 20°.

the path followed by the black line. For values of $Q_1 > 1.1$ the pole is within a region bounded by the principal axes associated with the primary and secondary loads, respectively; in this situation, the primary load continues to push the pole toward the equator, while the secondary load (and remnant rotational bulge) resist this trend. At $Q_1 \sim 1.31$, the pole experiences a major instability defined by a 90° shift away from this great circle. This instability is an IITPW event. In this scenario, since $\theta_1 \neq 0$, the primary load is unable to perfectly cancel the nonhydrostatic remnant

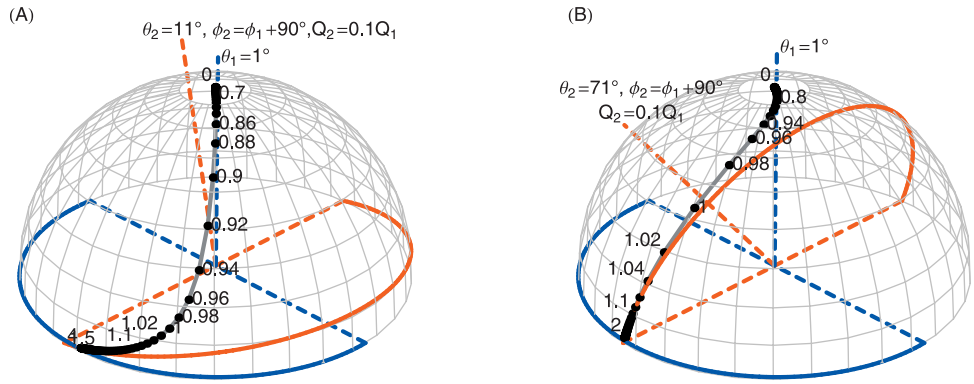

Figure 7. Predicted TPW for the nonaxisymmetric load scenario shown by Case 2 in Figure 5 (i.e., the great circles connecting the initial pole location to the primary and secondary loads are perpendicular). In both frames $Q_2 = 0.1\ Q_1$ and $\theta_1 = 1°$, and the black line joins results for a sequence of progressively larger values of Q_1 (as labeled). The frames are distinguished on the basis of the position of the secondary load: (a) $\theta_2 = 11°$ or (b) $\theta_2 = 71°$.

rotational bulge; however, the additional inertia tensor contribution from the secondary load makes such a cancellation possible. Note that for values of $Q_1 > 1.31$ the pole position is stable and located at the intersection of the equatorial great circles (red and blue lines) defined by the two loads. As discussed above, the "residual" effective loads (that is, the effective loads after removal of the portion that cancels the remnant rotational bulge), no matter their size, will govern the location of the pole.

[57] As in the axisymmetric case, we can write expressions for the inertia tensor perturbations, diagonalize the tensor and derive conditions for both the equilibrium pole location and IITPW. Lengthy algebra yields the following condition for the pole location and the point at which an equality between I_{22} and I_{33} is achieved,

$$\begin{aligned} Q_1 \sin\left(2\theta_1^f\right) + Q_2 \sin\left(2\theta_2^f\right) &= \sin(2\delta) \\ Q_1 \cos^2\left(\theta_1^f\right) + Q_2 \cos^2\left(\theta_2^f\right) &= \cos^2(\delta). \end{aligned} \tag{38}$$

Simultaneous solution of these equations can be used to predict the effective load magnitude (Q_1) and the colatitude (measured from the original pole location) at which the IITPW event occurs.

[58] The remaining frames on the top row of Figure 6 show summary results for cases in which θ_1 is varied up to 5° and the secondary load is either 10% (as above) or 20% of the primary load. We retain the 10° shift between load centers. The middle frame shows the Q_1 value necessary for an IITPW event, and the right frame shows the colatitude at which the event will occur. The main point in these results is that as the primary load is moved away from the original pole, the size of the load required to initiate an IITPW event grows rapidly. Indeed, in the case of $\theta_1 = 5°$ and $Q_2 = 0.1Q_1$, a value $Q_1 = 4.7$ is required to initiate an IITPW event.

[59] In the bottom frames of Figure 6 we consider a second Case 1 scenario in which the displacement between the primary and secondary loads is increased to 70°. For $\theta_1 = 1°$ and $Q_2 = 0.1Q_1$, a Q_1 value above 0.97 will bring the rotation pole into a region within the great circles perpendicular to the two load axes (left frame). Furthermore, in the same case, a value of $Q_1 = 1.02$ initiates an IITPW event at a colatitude of ~30°. As θ_1 is increased up to 20° (middle and right frames), the Q_1 value necessary for the onset of IITPW increases to just 2.4, while the colatitude at which the instability occurs increases to ~55°. These values drop to 1.8 and 45°, respectively, when $Q_2 = 0.2\ Q_1$. Clearly, given some upper bound on the size of the primary load, a larger displacement between the primary and secondary loads yields a broader range of load locations that may yield an IITPW event.

[60] In Figure 7 we turn our attention to the Case 2 scenario of Figure 5, and show a sequence of results (for increasing Q_1) for $\theta_1 = 1°$ and a displacement between loads of either 10° (Figure 7a) or 70° (Figure 7b). In this case, the secondary load acts to deflect the pole location off the great circle joining the initial pole and the primary load. The size of this deflection decreases as the displacement between the primary and secondary loads increases since the great circle perpendicular to the secondary load axis comes into closer alignment with the great circle joining the initial pole and primary load (compare the red great circles in Figures 7a and 7b). As the size of the primary load (Q_1) is increased, the pole first moves off the latter great circle, but eventually returns toward this great circle. The pole returns to this longitude since it is where the great circles that are perpendicular to the load axes intersect. Consider the $\theta_2 = 11°$ scenario (Figure 7a), for values of $Q_1 \sim 1.5$, the equilibrium pole position has reached close to the point of intersection between the two great circles that are perpendicular to the load axes. In contrast, for $Q_1 \lesssim 0.92$, the pole will be deflected ~45° from this longitude. In any event, the Case 2 scenario does not produce an IITPW instability; that is, the positioning of the loads along perpendicular trajectories from the initial rotation pole (Figure 5) will not lead to a situation where the maximum and intermediate nonhydrostatic moments of inertia become equal.

[61] These scenarios are highly simplified, but they provide significant insight into the connection between load asymmetry and rotational stability. The main result is that even small levels of asymmetry can profoundly influence the rotational stability. For components of asymmetry aligned with the great circle joining the initial pole and the primary load, this impact includes the potential initiation of IITPW events.

3. Impact of Internally Supported Inertia Perturbations

[62] In this section we augment the theory outlined above to include perturbations in the inertia tensor dynamically supported by internal, convective motions (Figures 1g–1i). Few, if any, constraints currently exist on the amplitude and/or orientation of internal convective motions on planets other than Earth. Accordingly, the mathematics outlined below is, by necessity, general.

[63] We begin by assuming the total gravitational potential perturbation associated with internal convective flow (including the mass heterogeneity and its induced surface deformation) is known. If we denote these harmonics by $\mathcal{G}_{\ell m}^{INT}(t)$ then equation (3) gives

$$\begin{aligned} I_{11}^{INT}(t) &= \frac{Ma}{g}\left[\frac{\sqrt{5}}{3}\mathcal{G}_{20}^{INT}(t) - 2\sqrt{\frac{5}{6}}\mathrm{Re}\left(\mathcal{G}_{22}^{INT}(t)\right)\right], \\ I_{22}^{INT}(t) &= \frac{Ma}{g}\left[\frac{\sqrt{5}}{3}\mathcal{G}_{20}^{INT}(t) + 2\sqrt{\frac{5}{6}}\mathrm{Re}\left(\mathcal{G}_{22}^{INT}(t)\right)\right], \\ I_{33}^{INT}(t) &= -\frac{2\sqrt{5}}{3}\frac{Ma}{g}\mathcal{G}_{20}^{INT}(t), \\ I_{12}^{INT}(t) &= 2\sqrt{\frac{5}{6}}\frac{Ma}{g}\mathrm{Im}\left(\mathcal{G}_{22}^{INT}(t)\right), \\ I_{13}^{INT}(t) &= 2\sqrt{\frac{5}{6}}\frac{Ma}{g}\mathrm{Re}\left(\mathcal{G}_{21}^{INT}(t)\right), \\ I_{23}^{INT}(t) &= -2\sqrt{\frac{5}{6}}\frac{Ma}{g}\mathrm{Im}\left(\mathcal{G}_{21}^{INT}(t)\right), \end{aligned} \tag{39}$$

where we have assumed that the degree zero potential harmonic is zero. We remind the reader that the spherical harmonic decomposition will be based on a reference frame in which the north pole refers to the initial rotation axis (i.e., the rotation axis that defines the orientation of the remnant rotational bulge).

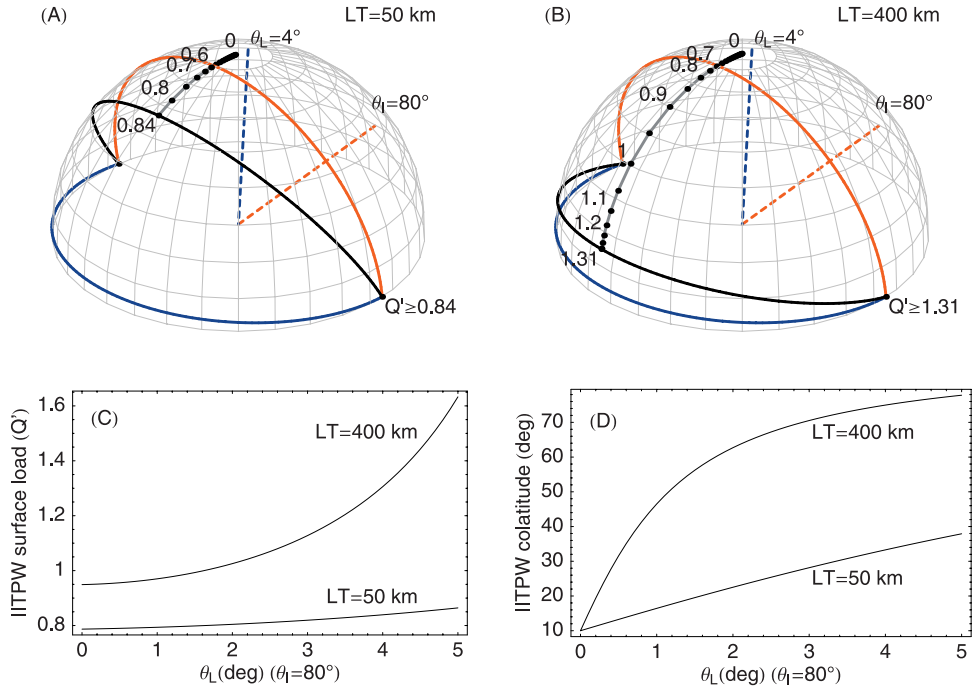

Figure 8. TPW driven by a combination of surface mass and internal loading. The internal load is fixed, and is characterized by an excess ellipticity which is 1% of the hydrostatic bulge of the planet ($Q'' = 0.01$). The principal axis for this component is given by the dashed red line ($\theta_I = 80°$); the great circle perpendicular to this axis is given by the solid red line. (top) Predicted pole positions for the case where the surface mass load has an initial colatitude $\theta_L = 4°$ and Q' is varied (as labeled). The frames are distinguished by the choice of lithospheric thickness: (a) 50 km or (b) 400 km. (c) The effective surface load size (Q') required to produce an IITPW event, as well as (d) the colatitude of the pole when this event is initiated, as a function of the initial load colatitude θ_L. Figures 8c and 8d show results for LT = 50 km and 400 km.

[64] In this case, the total inertia tensor perturbation is

$$I_{ij}(t) = I_{ij}^{L} + I_{ij}^{L-D} + I_{ij}^{ROT} + I_{ij}^{INT}(t), \tag{40}$$

where a general expression for the first three terms on the right hand side is given by equation (21). Note that we retain the time dependence in the evolving contribution from convective flow but we continue to assume that the timescale associated with this flow is much longer than the decay times that govern the viscous adjustment of the rotational bulge. We also assume that the geoid/inertia contributions from convective motions, if they were to be computed using viscous flow calculations, would involve an elastic lithosphere with thickness consistent with the remaining terms in equation (40).

[65] At this point, we can consider a special case. As in the treatment of the surface mass disk load, let us assume that gravitational potential associated with internal flow is axisymmetric relative to a geographic point (θ_I, ϕ_I). Let us furthermore denote the degree two zonal component of the potential (in a reference frame in which the axis of symmetry is at the pole) by $\mathcal{G}_{20}^{\prime INT}(t)$. Then, in analogy with equation (22), we have

$$\mathcal{G}_{2m}^{INT}(t) = \mathcal{G}_{20}^{\prime,INT}(t)\frac{Y_{2m}^{\dagger}(\theta_I,\phi_I)}{\sqrt{5}}. \tag{41}$$

If we furthermore normalize this signal relative to the potential perturbation associated with the hydrostatic rotational bulge,

$$Q''(t) = -\frac{\mathcal{G}_{20}^{\prime,INT}(t)}{\frac{-1}{3\sqrt{5}}a^2\Omega^2 k_f^{T*}}, \tag{42}$$

then equation (39) becomes

$$\begin{aligned}
I_{11}^{INT}(t) &= \frac{1}{3}m'Q''(t)\beta\left[\frac{1}{\sqrt{5}}Y_{20}(\theta_I) - \sqrt{\frac{6}{5}}\mathrm{Re}\left(Y_{22}^{\dagger}(\theta_I,\phi_I)\right)\right],\\
I_{22}^{INT}(t) &= \frac{1}{3}m'Q''(t)\beta\left[\frac{1}{\sqrt{5}}Y_{20}(\theta_I) + \sqrt{\frac{6}{5}}\mathrm{Re}\left(Y_{22}^{\dagger}(\theta_I,\phi_I)\right)\right],\\
I_{33}^{INT(t)} &= -\frac{2}{3}m'Q''(t)\beta\frac{1}{\sqrt{5}}Y_{20}(\theta_I),\\
I_{12}^{INT}(t) &= \frac{1}{3}m'Q''(t)\beta\sqrt{\frac{6}{5}}\mathrm{Im}\left(Y_{22}^{\dagger}(\theta_I,\phi_I)\right),\\
I_{13}^{INT}(t) &= \frac{1}{3}m'Q''(t)\beta\sqrt{\frac{6}{5}}\mathrm{Re}\left(Y_{21}^{\dagger}(\theta_I,\phi_I)\right),\\
I_{23}^{INT}(t) &= -\frac{1}{3}m'Q''(t)\beta\sqrt{\frac{6}{5}}\mathrm{Im}\left(Y_{21}^{\dagger}(\theta_1,\phi_1)\right),
\end{aligned} \tag{43}$$

where

$$\beta = \frac{1}{1 - k_f^T / k_f^{T*}}. \tag{44}$$

[66] In applying equation (40), the appropriate expression for I_{ij}^{INT} above may be combined with previous expressions we derived for the inertia tensor contribution from surface mass loading. As a simple example, Figure 8 provides a sample of the application of these governing equations. In particular, we predict the equilibrium rotational state for the case of a planet subject to both internal and external loading. In the top frames, the amplitude of the surface mass load (Q', rather than Q_{eff}) is varied and its initial load colatitude is fixed to $\theta_L = 4°$. The internal load is oriented so that the principal axis of this perturbation lies at $\theta_I = 80°$ along the same great circle joining the rotation pole and surface mass load; the amplitude is fixed to an excess ellipticity 1% of the hydrostatic bulge of the planet. That is, $Q'' = 0.01$. Figures 8a and 8b are distinguished on the basis of the lithospheric thickness adopted in the calculations (for the five-layer model of Martian structure described by *Bills and James* [1999]). The strong dependence on LT apparent on the figure arises because the total convection signal is imposed, a priori, while the remnant rotational bulge is a function of the lithospheric thickness. (We note that in Figures 6 and 7 the LT dependence is embedded in the value for the effective load, $Q_{eff} = Q'\alpha$, used on the figure; as we have discussed, since both the surface load and bulge adjustment are subject to compensation that is a function of LT, the balance associated with these two processes has a weaker sensitivity to LT.) As in the case of the two surface mass loads of Figure 6, the pole experiences an IITPW event when the combination of the surface and internal loads overcome the stabilizing effect of the remnant rotational bulge.

[67] The bottom frames in Figure 8 show (Figure 8c) the surface load size (Q') required for an IITPW event (we remind the reader that the internal load magnitude is fixed at $Q'' = 0.01$ for these tests), and (Figure 8d) the pole colatitude at which this instability occurs, as a function of the initial surface load colatitude. As the lithosphere thins, the remnant rotational fossil bulge and uncompensated component of the surface mass load diminish. The impact of the fixed convection signal on the rotational state thus increases. The net effect is that an IITPW event is initiated for smaller values of the surface load and the colatitude at which the event occurs decreases. In any event, the main conclusion for this test is that relatively small ($Q'' = 0.01$) convection signals can, like the secondary surface mass loads applied in Figures 6 and 7, exert a significant control on TPW, including the initiation of IITPW events.

[68] To complete this section, we consider the special case of inertia tensor perturbations induced by internal, convective motions alone (i.e., in the absence of surface loading effects). The governing expressions for this case are given by

$$I_{ij}^{INT,ROT}(t) = I_{ij}^{INT}(t) + I_{ij}^{ROT}, \tag{45}$$

where equations (24) (with $Q' = 0$) and (39) yield

$$\begin{aligned}
I_{11}^{INT,ROT}(t) &= \frac{Ma}{g}\left[\frac{\sqrt{5}}{3}\mathcal{G}_{20}^{INT}(t) - 2\sqrt{\frac{5}{6}}\mathrm{Re}\left(\mathcal{G}_{22}^{INT}(t)\right)\right] - \frac{1}{3}m', \\
I_{22}^{INT,ROT}(t) &= \frac{Ma}{g}\left[\frac{\sqrt{5}}{3}\mathcal{G}_{20}^{INT}(t) + 2\sqrt{\frac{5}{6}}\mathrm{Re}\left(\mathcal{G}_{22}^{INT}(t)\right)\right] - \frac{1}{3}m', \\
I_{33}^{INT,ROT}(t) &= -\frac{2\sqrt{5}}{3}\frac{Ma}{g}\mathcal{G}_{20}^{INT}(t) + \frac{2}{3}m', \\
I_{12}^{INT,ROT}(t) &= 2\sqrt{\frac{5}{6}}\frac{Ma}{g}\mathrm{Im}\left(\mathcal{G}_{22}^{INT}(t)\right), \\
I_{13}^{INT,ROT}(t) &= 2\sqrt{\frac{5}{6}}\frac{Ma}{g}\mathrm{Re}\left(\mathcal{G}_{21}^{INT}(t)\right), \\
I_{23}^{INT,ROT}(t) &= -2\sqrt{\frac{5}{6}}\frac{Ma}{g}\mathrm{Im}\left(\mathcal{G}_{21}^{INT}(t)\right),
\end{aligned} \tag{46}$$

where m' is defined in equation (25).

[69] These equations raise an interesting issue. In geophysical studies of the Earth's history of TPW [e.g., *Spada et al.*, 1992, 1996; *Ricard et al.*, 1993; *Richards et al.*, 1997, 1999; *Steinberger and O'Connell*, 1997; *Greff-Leftz*, 2004] it has been assumed, following the arguments by *Gold* [1955] and *Goldreich and Toomre* [1969], that the rotational bulge of the Earth will ultimately respond hydrostatically to a change in the orientation of the rotation vector. (This hydrostatic adjustment is either imposed, a priori, or it is embedded in the long-timescale, secular, limit of the governing stability equations.) That is, the assumption is made that there is no remnant rotational flattening (i.e., $m' = 0$). However, the development of the Earth's lithosphere implies that a nonzero remnant rotational bulge may contribute to the rotational stability. As discussed above, the exact nature of this remnant bulge may be more complicated than equation (46) implies. Since most studies of the Earth's long-term TPW have been concerned with the recent (last $\sim$100 Ma) geological record, the remnant bulge would reflect an integration of the incremental changes in some globally averaged "effective" lithospheric strength oriented with reference to the contemporaneous location of the rotation pole. Moreover, the impact of plate tectonics on this effective strength would clearly have to be considered. Furthermore, if one found that the timescale of lithospheric relaxation (say τ) was much smaller than the age of the Earth, then convection-induced TPW over the last 100 Ma would be impacted by the presence of a lithosphere only for timescales of mantle flow that are shorter than τ (i.e., only for timescales in which the lithosphere retains some effective elastic strength).

4. Final Remarks

[70] We have adopted the fluid limit of viscoelastic Love number theory to investigate the rotational stability of dynamic planets characterized by long-term (elastic) lithospheric strength. Our theoretical development treats the compensation of surface mass loads independently of the adjustment of the rotational bulge (through k_f^L and k_f^T Love numbers, respectively), and we conclude, in contrast to *Willemann* [1984], that the equilibrium position of the

rotation vector is a function of the lithospheric thickness (LT). Using fluid Love numbers computed for a model of Martian structure, we find that the TPW driven by axisymmetric surface mass loading is progressively larger than *Willemann*'s [1984] predictions as the lithosphere is thinned (Figure 4); indeed, the predictions only converge for LT values greater than ~400 km.

[71] Our analysis of TPW driven by axisymmetric loads, summarized in Figures 2 and 3, bridges results from earlier, classic studies of *Gold* [1955] and *Willemann* [1984]. As an example, *Gold* [1955] argued that TPW on a hydrostatic planet (i.e., a planet in which the rotational bulge will eventually reorient perfectly to a change in pole position) will ultimately move any uncompensated surface mass load to the equator. In the case of a planet with an elastic lithosphere, both the surface mass load and the rotational bulge will experience incomplete compensation. For such a planet, a reorientation of the load to the equator will occur in two situations (see Figure 2): (1) when the surface mass load is extremely large (i.e., $Q_{eff} \gg 1$) or (2) when a load which exceeds the size of the remnant rotational bulge ($Q_{eff} > 1$) is placed at the initial pole position. In the latter case, the remnant rotational bulge is "canceled" by the component of the surface mass load up to $Q_{eff} = 1$ and the residual (i.e., a load component of any size in excess of $Q_{eff} = 1$) will drive an IITPW instability.

[72] We have also extended *Willemann*'s [1984] analysis to consider the impact of nonaxisymmetric surface mass loads and arbitrary, convectively supported contributions to the nonhydrostatic inertia tensor, on predicted TPW paths. We find that these contributions can exert a profound influence on the rotational stability (Figures 6–8). For example, surface mass load asymmetry modeled by including a secondary load along the same great circle joining the primary (axisymmetric) load and the initial rotation pole (Case 1 in Figure 5) is capable of inducing an IITPW event. We have derived the stability conditions governing this event (see equations 38); for a given upper bound on the size of the effective surface load, a larger displacement between the primary and secondary loads increases the range of load locations that can give rise to IITPW (Figure 6). In contrast, load asymmetries modeled by incorporating a secondary load in a location perpendicular to the great circle joining the primary load and the initial rotation pole (Case 2 in Figure 5) act to deflect the pole from this great circle. The level of deflection depends on the size and location of the primary and secondary loads; we note from Figure 7 that moving the secondary load closer to the initial rotation pole acts to increase the excursion of the rotation vector from the great circle.

[73] The impact on the rotational dynamics of convectively induced perturbations in the planetary shape (Figure 8) can be understood in these same terms, since such contributions can be expressed as equivalent uncompensated components of the surface mass load. That is, the divergence of the pole position from simple TPW paths predicted on the basis of an axisymmetric surface mass load will depend on the magnitude and orientation (relative to the initial pole and axisymmetric surface load) of the convection signal.

[74] We conclude that the rotational stability of planets will be overestimated by analyses which are limited to simple axisymmetric loads of the type introduced by *Willemann* [1984] (and treated in our Figures 2–4). The TPW on Mars driven by Tharsis, an example discussed at various stages through this article, warrants several comments in this regard. First, our correction of *Willemann*'s [1984] theory for axisymmetric loads yields a broader range of TPW scenarios for a Tharsis-sized load (Figure 4) in the case of a relatively thin elastic lithosphere at the time of Tharsis formation. Second, in contrast to previous assertions, the equations governing the rotational stability permit a large (>65°) excursion of the Martian rotation pole in consequence of an axisymmetric Tharsis-sized loading (Figure 4). Third, asymmetries in the surface mass loading, either due to Tharsis structure or the presence of secondary loads (e.g., Elysium) on Mars, or contributions to the nonhydrostatic inertia tensor from convective processes, will introduce potentially large pole excursions off the great circle joining the initial rotation pole and the main Tharsis load. Indeed, these excursions may include an IITPW event.

[75] Finally, we note that the Love number theory described herein assumes a viscoelastic planetary model with a single, uniform elastic plate. A new generation of finite element models have been developed to consider the response of 3-D Earth models to generalized loading [e.g., *Wu and van der Wal*, 2003; *Zhong et al.*, 2003; *Latychev et al.*, 2005]. In future work, we will use such models to investigate the impact of plate boundaries and thickness variations on the computed rotational stability. These results will be used to reassess predictions of TPW on Earth over the last 100 Myr (see the discussion below equation (46)) and TPW driven by Tharsis loading in the event of tectonic activity on early Mars.

Appendix A: Load-Induced Geopotential Perturbations

[76] The geopotential perturbation associated with surface loading can be written as a space-time convolution of the viscoelastic Green's function for the geopotential anomaly with the surface mass load, $L(\theta, \phi, t)$,

$$\mathcal{G}(\theta,\phi,t) = \int_{-\infty}^{t} \int_{S} L(\theta',\phi',t') \cdot GF(\gamma, t-t') dS' dt', \qquad \text{(A1)}$$

where S represents the surface of the unit sphere, GF is the Green's function and γ is the angular distance from (θ, ϕ) to (θ', ϕ') given by

$$\cos\gamma = \cos\theta\cos\theta' + \sin\theta\sin\theta'\cos(\phi - \phi'). \qquad \text{(A2)}$$

We note that on a spherically symmetric planet, the response is dependent on the angular distance from the load and independent of azimuth. The viscoelastic Green's Function associated with the geopotential is given by [*Mitrovica and Peltier*, 1989]

$$GF(\gamma,t) = \frac{ag}{M}\sum_{\ell=0}^{\infty}\left[\delta(t) + k_{\ell}^{L}(t)\right]P_{\ell}(\cos\gamma), \qquad \text{(A3)}$$

where P_ℓ is the unnormalized Legendre polynomial at degree ℓ. In the square brackets on the right-hand-side of

equation (A3), the delta function refers to the direct effect of the surface mass load, while the Love number $k_\ell^L(t)$ (see equation (4)) accounts for the planetary deformation associated with this load.

[77] Using the normalization we have adopted (see equation (2)), the addition theorem of spherical harmonics yields

$$\int_S L(\theta',\phi')P_\ell(\cos\gamma)dS' = \frac{4\pi a^2}{2\ell+1}\sum_{m=-\ell}^{\ell} L_{\ell m}(t)Y_{\ell m}(\theta,\phi). \quad \text{(A4)}$$

Next, we apply equation (A3) in equation (A1) and use equation (A4) to perform the spatial convolution analytically. For each harmonic coefficient we obtain

$$\mathcal{G}_{\ell m}(t) = \frac{4\pi a^3 g}{M(2\ell+1)}L_{\ell m}(t) * \left[\delta(t) + k_\ell^L(t)\right], \quad \text{(A5)}$$

where the asterisk denotes a time convolution. In general we will be interested in load-induced perturbations at degree two, and in this case we can write

$$\mathcal{G}_{2m}(t) = \frac{4\pi a^3 g}{5M}L_{2m}(t) * \left[\delta(t) + k_2^L(t)\right]. \quad \text{(A6)}$$

It will be instructive to separate the perturbation into components associated with the direct mass attraction of the surface load and the deformation induced by this surface load (since, as we discussed in the main text, these are commonly thought of as two of the three contributions to changes in the inertia tensor components). If we denote these terms by the superscript L and $L - D$, respectively, we have

$$\mathcal{G}_{2m}^L(t) = \frac{4\pi a^3 g}{5M}L_{2m}(t) * \delta(t) = \frac{4\pi a^3 g}{5M}L_{2m}(t) \quad \text{(A7)}$$

$$\mathcal{G}_{2m}^{L-D}(t) = \frac{4\pi a^3 g}{5M}L_{2m} * k_2^L(t), \quad \text{(A8)}$$

where $\mathcal{G}_{2,-m}(t) = (-1)^m\mathcal{G}_{2m}^\dagger(t)$. In the limit of infinite time after the application of the surface mass load, these equations yield the expressions (6) and (7) within the main text.

[78] **Acknowledgments.** The authors thank David Stevenson and the Associate Editor for constructive reviews. We also thank David Stevenson and Victor Tsai for providing us with a copy of their manuscript prior to publication. We acknowledge support from the Canadian Institute for Theoretical Astrophysics, the Miller Institute for Basic Research, the Canadian Institute for Advanced Research, NSERC, and the NASA Astrobiology Institute.

References

Arkani-Hamed, J. (2005), Giant impact basins trace the ancient equator of Mars, *J. Geophys. Res.*, *110*, E04012, doi:10.1029/2004JE002343.

Arkani-Hamed, J., and D. Boutin (2004), Paleomagnetic poles of Mars: Revisited, *J. Geophys. Res.*, *209*, E03011, doi:10.1029/2003JE002229.

Banerdt, W. B., M. P. Golombek, and K. L. Tanaka (1992), Stress and tectonics on Mars, in *Mars*, edited by H. H. Kieffer et al., pp. 249–297, Univ. of Ariz. Press, Tucson.

Bills, B. G., and T. S. James (1999), Moments of inertia and rotational stability of Mars: Lithospheric support of subhydrostatic rotational flattening, *J. Geophys. Res.*, *104*, 9081–9096.

Gold, T. (1955), Instability of the Earth's axis of rotation, *Nature*, *175*, 526–529.

Goldreich, P., and A. Toomre (1969), Some remarks on polar wandering, *J. Geophys. Res.*, *74*, 2555–2567.

Greff-Leftz, A. (2004), Upwelling plumes, superwells and true polar wander, *Geophys. J. Int.*, *159*, 1125–1137.

Grimm, R. E., and S. C. Solomon (1986), Tectonic tests of proposed polar wander paths for Mars and the moon, *Icarus*, *65*, 110–121.

Lambeck, K. (1980), *The Earth's Variable Rotation: Geophysical Causes and Consequences*, Cambridge Univ. Press, New York.

Latychev, K., J. X. Mitrovica, J. Tromp, M. E. Tamisiea, D. Komatitsch, and C. Christara (2005), Glacial isostatic adjustment on 3-D Earth models: A new finite-element formulation, *Geophys. J. Int.*, *161*, 421–444.

Mitrovica, J. X., and W. R. Peltier (1989), Pleistocene deglaciation and the global gravity field, *J. Geophys. Res.*, *94*, 13,651–13,671.

Mitrovica, J. X., J. Wahr, I. Matsuyama, and A. Paulson (2005), The rotational stability of an ice-age Earth, *Geophys. J. Int.*, *161*, 491–506.

Peltier, W. R. (1974), The impulse response of a Maxwell Earth, *Rev. Geophys.*, *12*, 649–669.

Peltier, W. R. (1976), Glacial isostatic adjustment: 2. The inverse problem, *Geophys. J. R. Astron. Soc.*, *46*, 669–706.

Peltier, W. R., R. A. Drummond, and A. M. Tushingham (1986), Postglacial rebound and transient lower mantle rheology, *Geophys. J. R. Astron. Soc.*, *87*, 79–116.

Ricard, Y., G. Spada, and R. Sabadini (1993), Polar wandering of a dynamic Earth, *Geophys. J. Int.*, *113*, 282–298.

Richards, M. A., Y. Ricard, C. Lithgow-Bertelloni, G. Spada, and R. Sabadini (1997), An explanation for the long-term stability of Earth's rotation axis, *Science*, *275*, 372–375.

Richards, M. A., H. P. Bunge, and Y. Ricard (1999), Polar wandering in mantle convection models, *Geophys. Res. Lett.*, *26*, 1777–1780.

Schultz, P. H., and A. B. Lutz (1988), Polar wandering of Mars, *Icarus*, *73*, 91–141.

Spada, G., Y. Ricard, and R. Sabadini (1992), Excitation of true polar wander by subduction, *Nature*, *360*, 452–454.

Spada, G., R. Sabadini, and E. Boschi (1996), Long-term rotation and mantle dynamics of the Earth, Mars, and Venus, *J. Geophys. Res.*, *101*, 2253–2266.

Steinberger, B., and R. J. O'Connell (1997), Changes of the Earth's rotation axis owing to advection of mantle density heterogeneities, *Nature*, *387*, 169–173.

Steinberger, B., and R. J. O'Connell (2002), The convective mantle flow signal in rates of true polar wander, in *Ice Sheets, Sea Level and the Dynamic Earth*, *Geodyn. Ser.*, vol. 29, edited by J. X. Mitrovica and L. L. A. Vermeersen, pp. 233–256, AGU, Washington, D. C.

Ward, W. R. (1992), Long-term orbital and spin dynamics of Mars, in *Mars*, edited by H. H. Kieffer et al., pp. 298–320, Univ. of Ariz. Press, Tucson.

Willemann, R. J. (1984), Reorientation of planets with elastic lithospheres, *Icarus*, *60*, 701–709.

Wu, P., and W. R. Peltier (1984), Pleistocene deglaciation and the Earth's rotation: A new analysis, *Geophys. J. R. Astron. Soc.*, *76*, 753–792.

Wu, P., and W. van der Wal (2003), Postglacial sealevels on a spherical, self-gravitating viscoelastic Earth: Effects of lateral viscosity variations in the upper mantle on the inference of viscosity contrasts in the lower mantle, *Earth Planet. Sci. Lett.*, *211*, 57–68.

Zhong, S., A. Paulson, and J. Wahr (2003), Three-dimensional finite element modelling of Earth's viscoelastic deformation: Effects of lateral variations in lithospheric thickness, *Geophys. J. Int.*, *155*, 679–695.

Zuber, M. T., and D. E. Smith (1997), Mars without Tharsis, *J. Geophys. Res.*, *102*, 28,673–28,686.

I. Matsuyama, Department of Terrestrial Magnetism, Carnegie Institution of Washington, 5241 Broad Branch Road, NW, Washington, DC 20015-1305, USA. (matsuyama@dtm.ciw.edu)

J. X. Mitrovica, Department of Physics, University of Toronto, 60 St. George Street, Toronto, ON, Canada M5S 1A7.

M. Manga, J. T. Perron, and M. A. Richards, Department of Earth and Planetary Science, University of California, Berkeley, CA 94720-4767, USA.